Journal of Medicinal Chemistry

pubs.acs.org/jmc Article

Projected Dose Optimization of Amino- and Hydroxypyrrolidine Purine PI3Kδ Immunomodulators

Joey L. Methot,* Hua Zhou, Meredeth A. McGowan, Neville John Anthony, Matthew Christopher, Yudith Garcia, Abdelghani Achab, Kathryn Lipford, Benjamin Wesley Trotter, Michael D. Altman, Xavier Fradera, Charles A. Lesburg, Chaomin Li, Stephen Alves, Craig P. Chappell, Renu Jain, Ruban Mangado, Elaine Pinheiro, Sybill M. G. Williams, Peter Goldenblatt, Armetta Hill, Lynsey Shaffer, Dapeng Chen, Vincent Tong, Robbie L. McLeod, Hyun-Hee Lee, Hongshi Yu, Sanjiv Shah, and Jason D. Katz

Cite This: *J. Med. Chem.* 2021, 64, 5137−5156 Read Online

ACCESS | Metrics & More | Article Recommendations | Supporting Information

ABSTRACT: The approvals of idelalisib and duvelisib have validated PI3Kδ inhibitors for the treatment for hematological malignancies driven by the PI3K/AKT pathway. Our program led to the identification of structurally distinct heterocycloalkyl purine inhibitors with excellent isoform and kinome selectivity; however, they had high projected human doses. Improved ligand contacts gave potency enhancements, while replacement of metabolic liabilities led to extended half-lives in preclinical species, affording PI3Kδ inhibitors with low once-daily predicted human doses. Treatment of C57BL/6-Foxp3-GDL reporter mice with 30 and 100 mg/kg/day of **3c** (MSD-496486311) led to a 70% reduction in Foxp3-expressing regulatory T cells as observed through bioluminescence imaging with luciferin, consistent with the role of PI3K/AKT signaling in Treg cell proliferation. As a model for allergic rhinitis and asthma, treatment of ovalbumin-challenged Brown Norway rats with 0.3 to 30 mg/kg/day of **3c** gave a dose-dependent reduction in pulmonary bronchoalveolar lavage inflammation eosinophil cell count.

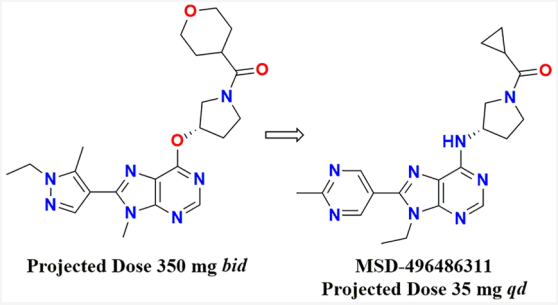

INTRODUCTION

Phosphoinositide 3-kinase delta (PI3Kδ) is expressed primarily in leukocytes where it regulates a broad range of cellular activities such as cell survival, proliferation, differentiation, and trafficking.[1] The lipid kinase converts PIP2 (phosphatidylinositol 4,5-bisphosphate) to PIP3 (phosphatidylinositol 3,4,5-trisphosphate), which in turn leads to the activation of the key regulatory kinase AKT. The role of PI3Kδ in B-cell activation has been investigated in hematologic malignancies driven by the AKT pathway, culminating in the 2014 approval of the selective PI3Kδ inhibitor idelalisib (Figure 1) for the treatment of follicular B-cell non-Hodgkin lymphoma, chronic lymphocytic leukemia, and small lymphocytic lymphoma.[2] This was followed by the approval of the structurally related PI3Kδ inhibitor duvelisib in 2019 for the treatment of hematological tumors.[3] Interestingly, Ali and colleagues have reported that inhibition of PI3Kδ in murine immunocompetent syngeneic models protects against a broad spectrum of cancers, including solid tumors with low expression of PI3Kδ.[4] This unexpected result may be due to an adaptive immune-mediated tumor surveillance response. Evaluation of PI3Kδ inhibition in non-oncology indications has been extensively studied as well. Resistance to inflammatory disease in genetically modified

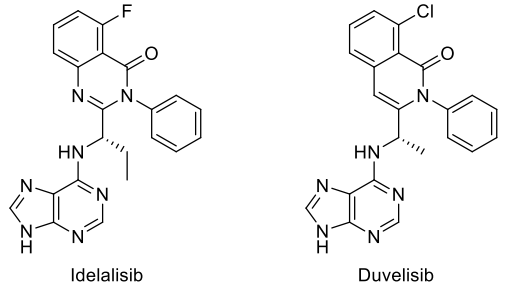

Figure 1. Approved inhibitors of PI3Kδ.

mice is consistent with involvement of PI3Kδ activity in dysregulated inflammatory responses. Taken together with the restricted expression and viability of PI3Kδ knock-out mice, PI3Kδ inhibitors have been considered for the treatment of

Received: February 6, 2021
Published: April 2, 2021

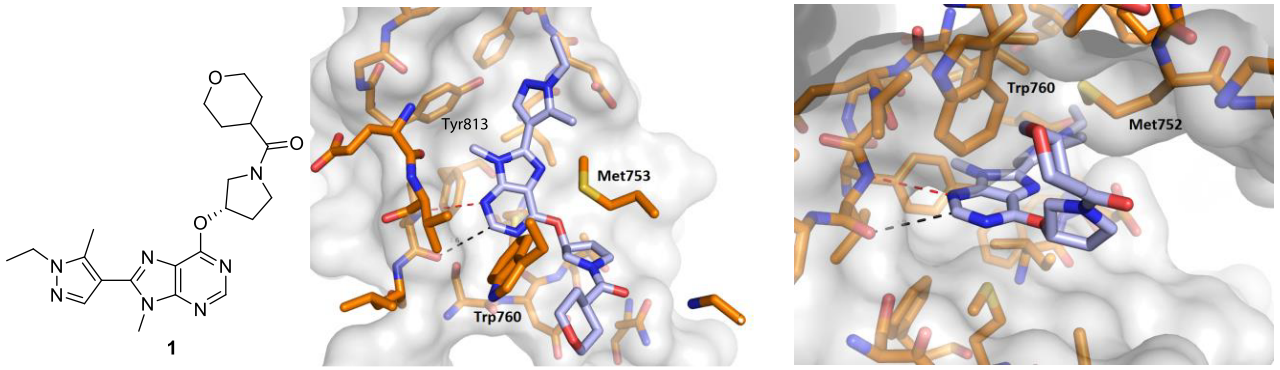

PI3Kδ IC_{50} (nM)	PI3Kα Sel.	pAKT IC_{50} (nM)	CD69 IC_{50} (nM)	CD63 IC_{50} (nM)	AdU IC_{50} (μM)	Papp[a] ($x10^{-6}$ cm/s)	HPLC LogD	Wistar Han Rat PK Profile				Beagle Dog PK Profile			
								Cl / Cl_{int} (mL/min/kg)	V_d / V_{du} (L/kg)	$t_{1/2}$ (h)	F (%)	Cl / Cl_{int} (mL/min/kg)	V_d / V_{du} (L/kg)	$t_{1/2}$ (h)	F (%)
3.9	69x	62	335	415	>10	12	1.1	41 / 126[b]	1.2 / 3.2	0.8	55	5.8 / 10[c]	0.9 / 1.1	1.5	100

Figure 2. Potency, PK profile, and crystal structure of **1** with PI3Kδ (3.05 Å). The purine makes hydrogen bond contacts to the kinase hinge region, while the pyrrolidine amide gears the tetrahydropyran toward the Trp760 residue. The purine N(9)-methyl is directed toward a cavity formed by gatekeeper Ile825 above and Tyr813 below. Unlike idelalisib and duvelisib, which induce a large hydrophobic pocket, the structure of bound **1** is similar to the apo form of the kinase. PDB ID: 6MUM. [a]LLC-PK1 cell line; [b]0.5 mg/kg *iv*, 1 mg/kg *po*; [c]0.25 mg/kg *iv*, 0.5 mg/kg *po* in DMSO/PEG400/H_2O-20/60/20; n = 2.

inflammatory conditions such as severe asthma, allergic rhinitis, COPD,[5] or activated PI3Kδ syndrome.[6] Preliminary studies with idelalisib in patients with allergic rhinitis demonstrated that PI3Kδ inhibition diminished total nasal symptom scores, nasal airflow, nasal secretion weights, and congestion.[7] Consequently, numerous organizations have reported PI3Kδ inhibitors to treat asthma and other inflammatory diseases, as well as liquid and solid tumors.[8,9]

In a previous communication, we described SAR studies that led to potent and selective pyrrolidine PI3Kδ inhibitor **1** by reconstruction of inhibitor XL-499.[10] As an early lead molecule, pyrrolidine **1** is structurally distinct from approved inhibitors idelalisib and duvelisib and has promising potency (PI3Kδ IC_{50} = 3.9 nM; LBE 0.36) and good to excellent selectivity versus PI3Kα (69x), PI3Kβ (1400x), and PI3Kγ (970x), as well as >1000× selectivity versus a 270-kinase panel. Kinases PI3Kα and PI3Kβ are ubiquitously expressed with roles in cell proliferation and metabolism, and genetic knockouts are embryonically lethal. Hence, we sought high selectivity versus PI3Kα and PI3Kβ, which have conserved ATP-binding sites.

The phosphorylation status of serine 473 of AKT in the Ramos Burkitt's lymphoma-derived B cell line is driven by PI3Kδ and is a measure of cellular activity of PI3Kδ inhibition (compound **1** AKT-pSer473 IC_{50} = 62 nM). Potency evaluation in human whole blood was used for clinical human dose prediction, in which we targeted the B-cell surface biomarker CD69 IC_{50} at trough concentration. CD69 is expressed in several hemopoietic cells as an early activation marker in chronic lymphocytic leukemia and is correlated with poor clinical prognosis.[11] In human whole blood, compound **1** inhibited anti-human CD79b-induced expression of the B-cell biomarker CD69 with an IC_{50} value of 335 nM.

The rat and dog PK profiles[12] for compound **1** are summarized in Figure 2. In rat, we observed a relatively short half-life (0.8 h), low intrinsic clearance (126 mL/min/kg), and good bioavailability (55%). In dogs, the half-life was also short (1.5 h); however, the intrinsic clearance was low (10 mL/min/kg) and the bioavailability was excellent (100%). In both species the volume of distributions were very low (V_{du} = 3.2 and 1.1 L/kg). While we did not detect significant turnover in microsome or hepatocyte incubations (Cl_{int} of <110 and <40 mL/min/kg, respectively), a rat bile duct cannulation of **1** indicated tetrahydropyran oxidation, pyrazole *N*-dealkylation, and cleavage of the ether bond. In addition, 17% of parent compound **1** was recovered in urine out to 24 h post-dose, with another 2% found in bile, suggesting a minor excretion contribution to the observed clearance.

Based on maintaining a C_{trough} concentration of 335 nM, the CD69 whole blood IC_{50} value, and the human PPB of only 17%, we predicted a human dose of 350 mg *bid* (human $t_{1/2}$ = 3 h, peak/trough = 9) using the allometry method for compound **1**. Such a high human dose could present a safety risk and prevent reaching higher levels of target engagement, if needed. We sought to lower the predicted human dose by improving both the potency and achieving a longer half-life in preclinical species. The generally low intrinsic clearance and unbound volume suggested that we could extend the half-life by addressing the metabolic liabilities identified in the rat bile duct cannulation study and by increasing the lipophilicity. We also needed to maintain the excellent kinome selectivity as well as selectivity over nonkinase off-targets such as adenosine uptake activity that plagued earlier inhibitors in this series.[13]

LEAD OPTIMIZATION

While the N(9)-methyl pyrazolopurine hinge-binding core served as a consistent platform to identify novel selectivity motifs leading to compound **1**, we understood little of the impact of purine C(8) and N(9) substitution on the potency, selectivity, and physical properties of this series. Furthermore, the pyrazole metabolism observed in the rat bile duct cannulation experiment with **1** suggested an alternative to the pyrazole that may lead to an improved half-life.

A portion of our SAR survey of this region of the molecule is shown in Table 1. Using the (*S*)-aminopyrrolidine ethyl amide selectivity motif, we first deleted the N(9)-methyl group; however, the corresponding inhibitor **2a** bearing an N-H lost 5× in potency versus the N(9)-methyl analog **2b** reference

https://doi.org/10.1021/acs.jmedchem.1c00237
J. Med. Chem. 2021, 64, 5137−5156

Table 1. Exploratory C(8)-Aryl and C(9)-Alkyl SAR with the (*S*)-Aminopyrrolidine Ethyl Amide Selectivity Motif

		PI3Kδ IC_{50} (nM)	PI3Kα Sel.	pAKT IC_{50} (nM)	AdU IC_{50} (μM)			PI3Kδ IC_{50} (nM)	PI3Kα Sel.	pAKT IC_{50} (nM)	AdU IC_{50} (μM)
2a	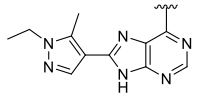	7.6	15x	875	5.4	2j	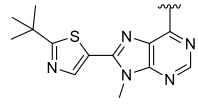	0.7	29x	4	1.6
2b	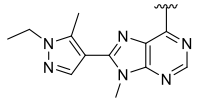	1.6	59x	24	7.3	2k	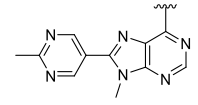	4.2	380x	71	2.0
2c	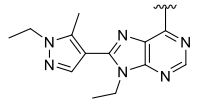	0.2	35x	2	2.3	2l	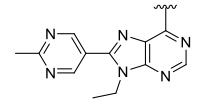	1.9	95x	42	
2d	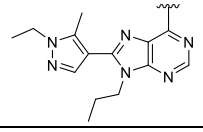	21	20x	198	3.7	2m	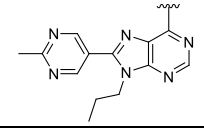	135	58x	455	
2e	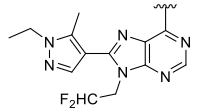	1.3	30x	14	3.1	2n	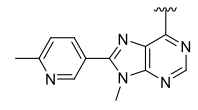	5.0	120x	160	3.8
2f	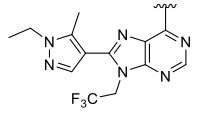	5.9	81x	330	9.3	2o	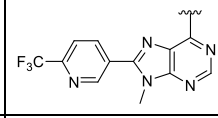	9.9	120x	66	0.7
2g	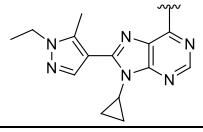	39	41x	720		2p	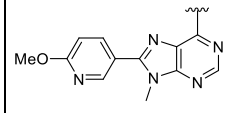	4.0	160x	67	1.9
2h	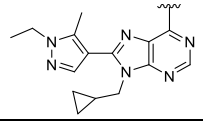	67	41x	1,350		2q	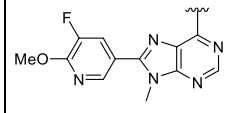	2.6	130x	20	1.3
2i	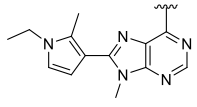	26	34x	125		2r	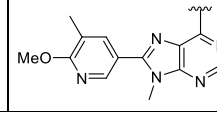	3.5	51x	6	0.3

analog (PI3Kδ IC_{50} = 1.6 nM). We next studied the impact of larger substituents at N(9) given the space available in the hydrophobic pocket lined by the gatekeepers Ile825 and Tyr813. The positioning of the gatekeeper residue above the plane of the hinge is unique to lipid kinases, creating a pocket between it and Tyr813 below the plane that can be exploited for potency and selectivity. Growing to an *N*-ethyl group (see **2c**) gave a nearly 10× boost in biochemical (PI3Kδ IC_{50} = 0.2 nM) and cellular potency relative to **2b**, while an *N*-propyl group (see **2d**) lost 10× in potency. This remarkable 100× span in potency from *N*-methyl to *N*-ethyl to *N*-propyl revealed not only the potency achievable with improved interaction with the gatekeeper Ile825 and Tyr813 but also the limited space available for larger substituents in the pocket. It is also noteworthy that the selectivity versus PI3Kα was consistent through the methyl−ethyl−propyl progression, which is not surprising given the high ATP site homology among the class I PI3Ks. For this series, selectivity versus PI3Kα was lower than other isoforms; hence, PI3Kα was chosen as a high-throughput indicator of selectivity.

With the exceptional potency exhibited by inhibitor **2c**, we profiled the inhibitor in rats and dogs. In rats, the clearance was moderate (Cl/Cl_{int} = 26/270 mL/min/kg) and the half-life was short (V_d = 0.9 L/kg, $t_{1/2}$ = 1.0 h; F = 52%). In dogs, the clearance was again moderate (Cl/Cl_{int} = 12/37 mL/min/kg) and the half-life was short (V_d = 1.3 L/kg, $t_{1/2}$ = 1.2 h; F = 100%). Compound **2c**, like **1**, was stable to liver microsomes. Furthermore, compound **2c** was a modest inhibitor of adenosine uptake in HeLa cells (IC_{50} = 2280 nM), while O-linked analog **1** was inactive in this assay (IC_{50} > 10,000 nM).

We continued to probe the SAR at C(9). Difluoroethyl **2e** was equipotent to the parent *N*-methyl-substituted **2b**; although less ligand-efficient, it may offer other advantages versus the *N*-methyl one. The larger trifluoromethyl group (**2f**) was less potent. Importantly, fluorinated analogs **2e** and **2f** had rat PK profiles very similar to **2c**, with comparable half-lives in rat and again stable to rat liver microsomes. The cyclopropyl

https://doi.org/10.1021/acs.jmedchem.1c00237
J. Med. Chem. 2021, 64, 5137−5156

Table 2. Pyrrolidine Amide Survey with the 2-Methylpyrimidine Purine

		L	PI3Kδ IC_{50} (nM)	PI3Kα Sel.	pAKT IC_{50} (nM)	CD69 IC_{50} (nM)	AdU IC_{50} (μM)	Papp[a] ($x10^{-6}$ cm/s)	HPLC LogD	Wistar Han Rat PK Profile				Beagle Dog PK Profile			
										Cl/Cl_{int} (mL/min/kg)	V_d/V_{du} (L/kg)	$t_{1/2}$ (h)	F (%)	Cl/Cl_{int} (mL/min/kg)	V_d/V_{du} (L/kg)	$t_{1/2}$ (h)	F (%)
3a	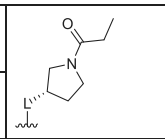	NH	1.9	95x	42		>10	21	0.7	21/100[b]	1.0/3.6	1.5	61	5.5/9.0[d]	1.5/1.9	2.7	
3b		O	13	220x			>10	21	0.8	12/31[d]	1.2/2.4	1.2		6.1/11[d]	1.9/2.7	3.9	
3c	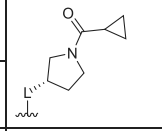	NH	1.3	160x	20	65	5.0	22	0.8	8.1/64[b]	1.0/6.3	2.7	55	4.3/6.2[c]	1.5/1.8	4.7	95
3d		O	5.9	170x	80	270	5.3	28	1.0	9.7/44[b]	0.7/2.8	1.8	64	4.9/7.0[c]	0.6/0.7	1.3	100
3e	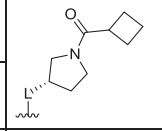	NH	0.4	160x	4	14	1.2	32	1.2	13/320[b]	0.5/9.2	0.6	74	11/30[c]	1.3/2.3	1.3	84
3f		O	1.2	530x	14		7.7		1.3	28/270[d]	0.6/4.0	0.3		12/27[d]	1.0/1.4	1.1	
3g	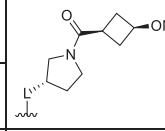	NH	0.8	120x	34	26	6.1	10	0.9	6.9/81[b]	1.5/4.1	2.3	52	7.1/13[c]	1.5/2.0	4.3	85
3h		O	2.8	480x	110	75	>10	18	1.0	3.8/19[b]	0.5/2.5	1.8	37	2.1/3.3[c]	0.6/0.9	3.6	80
3i	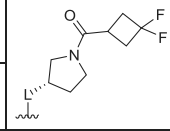	NH	2.2	68x	13		3.8		1.5	26/760[d]	0.9/18	0.4					
3j		O	3.8	290x	32	84	9.9		1.5	6.0/28[d]	0.5/3.0	1.4		23/170[d]	1.4/2.5	0.8	
3k	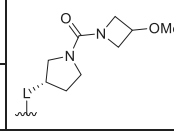	NH	0.7	150x	67	9.0	4.7	10	0.7	11/93[b]	0.7/4.8	4.0	16	9/19[c]	1.4/1.9	1.7	69
3l		O	3.3	180x	63		8.7		0.9	4.0/25[b]	0.4/2.1	1.7	75	12/32[d]	1.4/2.3	1.2	
3m	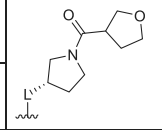	NH	1.6	140x			>10		0.6	18/74[d]	0.7/2.3	0.6					
3n		O	6.0	410x			>10		0.7	6.2/12[d]	0.5/0.9	1.4		3.0/4.2[d]	0.7/0.9	3.8	
3o	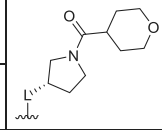	NH	2.1	86x	33		8.9	4.4	0.7	24/220[b]	0.7/4.3	1.4	18				
3p		O	13	88x	390		>10		0.8	14/37[b]	0.8/1.5	1.4	31	4.3/7.0[d]	0.8/1.1	1.9	
3q	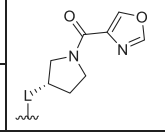	NH	2.8	65x	82				0.6	13/150[d]	0.6/6.1	0.7					
3r		O	6.4	140x	94	600	>10	21	0.7	3.7/25[b]	0.5/3.2	1.7	50	9.3/16[c]	1.7/1.9	1.8	100

[a]LLC-PK1 cell line. [b]0.5 mg/kg *iv*, 1 mg/kg *po*. [c]0.25 mg/kg *iv*, 0.5 mg/kg *po*. [d]0.05 mg/kg in DMSO/PEG400/H_2O-20/60/20; n = 2.

analogs **2g** and **2h** were likely too large for the space available and subsequently less potent than **2b**. Based on the crystal structures of **1** with PI3K*δ*, we suspected a direct or water-mediated contact between the pyrazole nitrogen and Tyr813. Hence, we prepared pyrrole **2i** and indeed observed a 16× loss in potency versus pyrazole **2b**, as expected. This one log unit potency shift is consistent with the loss of a hydrogen bond contact.

Given the *N*-dealkylation of the *N*-ethyl pyrazole ring of compound **1** observed *in vivo*, we explored alternative heterocycles that did not have an *N*-alkyl substituent. Potent thiazole **2j** (PI3K*δ* IC_{50} = 0.7 nM) bearing a *tert*-butyl substituent demonstrated not only the space available in the affinity pocket but also the potency gain achievable with a hydrophobic interaction. Not unexpectedly, thiazole **2j** had high clearance in rats ($Cl > Q_{hep}$). We turned to six-membered heterocycles commonly found in the literature as potency-enhancing motifs in the affinity pocket. 2-Methylpyrimidine **2k** was found to be 3× less potent than pyrazole **2b**; however, selectivity versus PI3K*α* improved from 60× to 375× with **2k**. With this improved selectivity, we explored the N(9) substituent, finding that N(9)-ethyl **2l** recovered the potency loss with this pyrimidine (PI3K*δ* IC_{50} = 1.9 nM) and maintained promising selectivity versus PI3K*α* (95×). As expected from our observations with **2b**−**2d**, N(9)-propyl-substituted **2m** was significantly less potent. Importantly, pyrimidine **2l** had superior rat and dog PK profiles versus the pyrazole analog **2c**, with intrinsic clearances 3× lower in both

https://doi.org/10.1021/acs.jmedchem.1c00237
J. Med. Chem. 2021, 64, 5137−5156

Table 3. Pyrrolidine Amide Survey with Trifluoromethyl Pyridine Purine

		PI3Kδ IC_{50} (nM)	PI3Kα Sel.	pAKT IC_{50} (nM)	CD69 IC_{50} (nM)	AdU IC_{50} (μM)	Papp[a] ($x10^{-6}$ cm/s)	HPLCL ogD	Wistar Han Rat PK Profile				Beagle Dog PK Profile			
									Cl/Cl_{int} (mL/min/kg)	V_d/V_{du} (L/kg)	$t_{1/2}$ (h)	F (%)	Cl/Cl_{int} (mL/min/kg)	V_d/V_{du} (L/kg)	$t_{1/2}$ (h)	F (%)
	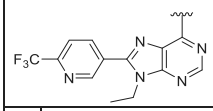															
4a	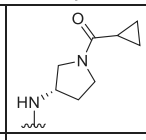	1.7	140x	12		1.2		2.0	4.7/104[b]	0.4/8.8	1.2	36	5.6/22[d]	1.2/3.9	3.1	
4b	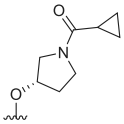	5.1	72x	49		5.6		2.3	15/240[d]	0.7/8.3	0.7					
4c	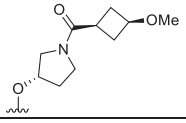	1.6	320x	67	73	4.1	35	2.2	3.6/130[b]	0.4/13	3.3	39	6.2/18[c]	1.1/2.5	2.6	100
4d	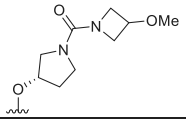	1.3	140x	43	68	2.2	33	2.1	1.7/29[b]	0.2/4.2	2.0	52	12/46[c]	0.7/1.7	0.7	100
4e	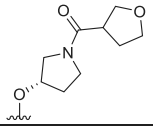	4.1	270x	110	100	3.2	27	1.9	1.2/19[b]	0.2/3.6	2.3	58	3.4/6.0[c]	0.9/1.6	3.6	100
4f	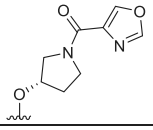	7.5	84x	300	380	4.4	29	2.0	1.3/13[b]	0.3/2.6	6.0	100	5.6/19[c]	1.2/3.4	2.5	100

[a]LLC-PK1. [b]0.5 mg/kg *iv*, 1 mg/kg *po*. [c]0.25 mg/kg *iv*, 0.5 mg/kg *po*. [d]0.05 mg/kg in DMSO/PEG400/H_2O-20/60/20; n = 2.

rats and dogs (Cl_{int} = 100, 9.0 mL/min/kg for **2l**), and an improved half-life (1.5−2.7 h for **2l**; note that **2l** is numbered **3a** in Table 2 where PK parameters are displayed). The low unbound volumes in rats and dogs for **2l** (V_{du} = 3.6, 1.9 L/kg) were comparable to the pyrazole series, suggesting that the improvements in the half-life were derived from lower intrinsic clearances.

To provide additional options for lead optimization, we identified 2-methylpyridine **2n** and 2-trifluoromethylpyridine **2o** at C(8), which can impact the physical properties of the series with one fewer aromatic nitrogen atom. A 2-methylpyridine ring has a cLogP of about 0.4 units above that of a 2-methylpyrimidine ring, while a 2-trifluoromethyl-pyridine ring has a cLogP of 1.0 unit above that of a 2-methylpyrimidine ring. This effect was readily apparent in HPLC-determined Log *D* values for pyrimidine **2k** (0.4), pyridines **2n** (0.8), and **2o** (1.6), demonstrating an opportunity to tune polarity and introduce nonmetabolizable lipophilicity as needed. For comparison, the 5-methyl-1-ethylpyrazole analog **2b** had a Log *D* value of 0.8. The added lipophilicity did render **2o** a more potent inhibitor of adenosine transport in HeLa cells (AdU IC_{50} = 0.7 μM for **2o**). The 2-methoxypyridine moiety is frequently used to gain potency in the affinity pocket of kinases, often through interactions with the Lys−Asp salt bridge. In our series, 2-methoxypyridine **2p** was no more potent than 2-methylpyridine **2n**. 3-Fluoro-2-methyoxypyridine **2q** and 3-methyl-2-methoxypyridine **2r** were slightly more potent than 2-methylpyridine **2n** in the enzyme assay but 8−25× more potent in the Ramos pAKT cell assay. Unfortunately, both **2q** and **2r** had high clearance in rats (Cl 69−71 mL/min/kg) and a short half-life ($t_{1/2}$ = 0.1 h), possibly due to metabolism of the 2-methoxypyridine ring. Furthermore, analogs bearing the 2-methoxypyridine motif was also more active in the HeLa cell adenosine transport assay (e.g., HeLa AdU IC_{50} = 0.3 μM for **2r**).

Based on the metabolism and *N*-dealkylation of the ethyl pyrazole ring observed in rat bile duct cannulation with inhibitor **1** and improvements in intrinsic clearance and the half-life observed when comparing **2c** with **2l**, we elected to continue lead optimization efforts with the 2-methylpyrimidine at C(8) of the purine instead of the pyrazole group. Furthermore, the boost in potency observed with the N(9)-ethyl group directed our efforts to this substituent versus the N(9)-methyl group.

The metabolism observed on the tetrahydropyran ring of compound **1** in a rat bile-duct cannulation study led us to explore alternative amides to improve the half-life in preclinical species. A small portion of the pyrrolidine amide cap SAR surveyed is outlined in Table 2, with both the NH linker as well as the O linker. Compound **2l** is listed first as a reference; compound **2l** is also **3a**. For reasons still unknown, the NH-linked pyrrolidine amides were frequently 4× more potent than the corresponding O-linked pyrrolidine amides. For example, O-linked ethyl amide **3b** is 6× less potent than the corresponding NH-linked analog, whereas with larger amides, this difference tends to be smaller. However, the O-linked analogs often offered improved selectivity versus PI3Kα kinase

https://doi.org/10.1021/acs.jmedchem.1c00237
J. Med. Chem. 2021, 64, 5137−5156

(compound **3b** selectivity is 220×; twice the selectivity of the NH-linked **3a**) and reduced adenosine uptake activity in HeLa cells. Furthermore, O-linked analogs occasionally had better half-lives in preclinical species. Hence, most pyrrolidine capping groups were explored with both the NH-linked and O-linked pyrrolidine series. Generally, amides bearing linear or branched alkyl chains (e.g., **3a**/**3b**) gave higher rat plasma clearances than small cycloalkyl amides. We identified numerous amide, urea, carbamate, and sulfonamide-linked capping groups on the pyrrolidine that maintained good to excellent enzymatic potency, with small aliphatic or heterocyclic groups being generally preferred over polar residues such as charged amines. The PI3Kδ potency SAR can be reviewed in the patent literature.[14] These diverse options for potency gave us an opportunity to broadly evaluate PK in rats and dogs to optimize for half-life in preclinical species. As noted earlier, in vitro models for metabolism (microsome, hepatocyte) were not predictive of the observed PK in rats or dogs, hence the need for in vivo screening. Generally, promising compounds with a rat half-life of 1.5 h or longer were further profiled. The volume of distribution was consistently low for this series (e.g., V_{du} = 3.6, 1.9 for **2l**/**3a**), necessitating a low intrinsic clearance to achieve an acceptable half-life of >1.5 h in rats.

Early in our amide screening campaign, we identified cyclopropyl amides **3c** and **3d**. The NH-linked **3c** was 4× more potent than O-linked **3d**; furthermore, **3c** offered better PK profiles. The pharmacokinetic properties of compound **3c** in rats and dogs were characterized by low plasma clearance (Cl of 8 and 4 mL/min/kg, respectively; with Cl_{int} of 64 and 6.2 mL/min/kg), good terminal half-life (2.7 and 4.3 h, respectively), and good bioavailability (55 and 95%, respectively). The unbound volume of distribution for **3c** (V_{du} = 6.3 and 1.8 L/kg in rats and dogs) is three-fold higher in rats than for ethyl amide **3a** but is unchanged in dogs versus **3a**, suggesting that the improved half-life in rats was at least partially driven by a larger unbound volume of distribution. Based on the allometry scaling method, the human pharmacokinetic properties of compound **3c** was predicted to be Cl of 3.8 mL/min/kg, V_d of 3.1 L/kg (V_{du} of 4.4 L/kg), $t_{1/2}$ of 9.0 h, and a bioavailability of 72%. To achieve a minimum blood concentration of 65 nM (the human whole blood CD69 IC_{50}), a dose of 35 mg once-daily will be required (see Table 4). To achieve a minimum blood concentration of 590 nM (the human whole blood CD69 IC_{90}), a dose of 260 mg once-daily or 76 mg twice-daily will be required. Given the high solubility, a dose number of <1 is expected.

Following the identification of cyclopropyl amide **3c**, we continued our SAR campaign to identify further optimized inhibitors, with longer predicted human half-lives. We placed simple methyl and fluoro substituents at various locations about the pyrrolidine and cyclopropane in an attempt to increase the unbound volume of distribution, identifying numerous equipotent analogs. However, the PK profiles of such close analogs were generally inferior to **3c**, with higher intrinsic clearances (see Supporting Information). We also attempted to increase the volume of distribution via the incorporation of basic amine substituents; however, half-lives were not improved. Finally, we sought to increase structural diversity in the series. For example, ring expansion of the cyclopropane to cyclobutyl amides **3e**/**3f** gave a 5× boost in potency versus the cyclopropyl analogs, presumably through improved van der Waals contacts with lipophilic residues Trp 760 and Met752. Unfortunately, the cyclobutyl amides also suffered from increased intrinsic clearances in both rats and dogs and consequently lower half-lives as well in both species, presumably due to increased amide metabolism since the unbound volumes were only slightly higher than **3c**. As expected, the HPLC Log *D* values increased by 0.3−0.4 units in expanding from the cyclopropyl amide to a cyclobutyl amide. To counter the effect of increased lipophilicity, we turned to substituents about the cyclobutane that may rebalance polarity with a lower Log *D*. For example, a *cis*-3-methoxy substituent brings the Log *D* closer to the original cyclopropyl amide. *cis*-3-Methoxycyclobutyl amides **3g** and **3h** were slightly less potent than cyclopropyl amides **3c** and **3d**; however, the low intrinsic clearances and excellent half-lives in rats and dogs were maintained ($t_{1/2}$ = 1.8−2.3 h in rats and 3.6−4.3 h in dogs). Once again, the improved half-lives were achieved by decreasing intrinsic clearance and not increasing unbound volume. Taken together, with the excellent human whole blood potency for these compounds (CD69 IC_{50} = 26 and 75 nM for **3g** and **3h**), human dose predictions based on the allometry approach were 40 mg *qd* with a P/T of 13 for **3g**, slightly inferior to **3c**, and 13 mg *qd* with a P/T of 4 for **3h**, slightly improved versus **3c** (Table 4). The strategy to rebalance the increased lipophilicity of a cyclobutane versus a cyclopropane with the polarity of an ether was successful in improving half-lives in rats and dogs. We also attempted to deactivate the cyclobutyl amide toward oxidative metabolism as well as increase the unbound volume of distribution with fluorine substitution, such as 3,3-difluorocyclobutyl amides **3i** and **3j**. The HPLC Log *D* values increased from 1.3 to 1.5; however, any gains in the unbound volume of distribution were nulled by increased intrinsic clearance, giving no improvement in rat or dog half-lives.

Encouraged by the promising human dose predictions for 3-methoxycyclobutyl amides **3g** and **3h**, we explored urea analogs **3k** and **3l**. Ureas were generally as potent as amides in biochemical, cell, and whole blood assays, and ureas **3k** and **3l** were no exception. However, the PK profiles had eroded significantly for ureas relative to the optimized amides above, with the best being urea **3k** ($t_{1/2}$ = 4, 1.7 h; bioavailability of 16

Table 4. Preliminary Human Dose Predictions Based on Maintaining B-Cell Activation Biomarker CD69 IC_{50}

				human dose prediction[b]		
compound	target[a] C_{trough} (nM)	human PPB (%)	unb'd target C_{trough} (nM)	dose (mg)	$t_{1/2}$ (h)	P/T[c]
1	335	17	280	350, *bid*	3	9
3c	65	28	47	35, *qd*	9	4
3c	590 (CD69 IC_{90} target)	28	430	260, *qd* (76, *bid*)	9	4
3d	270	38	100	285, *qd*	5	
3g	26	31	8	40, *qd*	5	13
3h	75	41	31	13, *qd*	10	4
3k	9	36	3	180, *qd*	5	27
4c	73	62	45	90, *qd*	6	10
4d	68	64	44	130, *qd*	4	43
4e	100	52	48	8, *qd*	10	4
4f	380	79	68	20, *qd*	10	4

[a]Human whole blood CD69 IC_{50} value unless otherwise noted. [b]Allometry approach using Tang's method, based on rat and dog PK data.[15] [c]Ratio of predicted C_{max}/C_{trough}.

https://doi.org/10.1021/acs.jmedchem.1c00237
J. Med. Chem. 2021, 64, 5137−5156

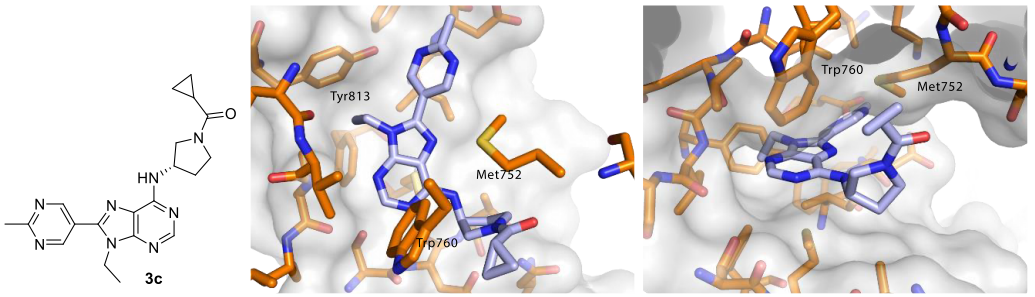

Potency and Selectivity

PI3Kδ IC_{50} (nM)	PI3Kα Sel.	PI3Kβ Sel.	PI3Kγ Sel.	Kinome Sel. n=280	pAKT IC_{50} (nM)	HWB CD69 IC_{50} (nM)	HWB CD63 IC_{50} (nM)	Mouse PI3Kδ IC_{50} (nM)	Rat PI3Kδ IC_{50} (nM)	Dog PI3Kδ IC_{50} (nM)
1.2	150x	1370x	3690x	100% >100x	20	65	50	2.2	6.6	2.5

Physical Properties and Safety Pharmacology

Stable Form	pH 7 Solubility	Papp[a] (x10^{-6} cm/s)	Human MDR1[b] PGP BA/AB	Human BCRP[b] BA/AB	hERG, Cav1.2, Nav1.5 IC_{50} (μM)	CYP-1A2, 2B6, 2C8, 3A4, 2C9, 2C19, 2D6 IC_{50} (μM)	CYP-3A4 TDI	Rat, Dog, Human Hep Cl_{int} (mL/min/kg)
crystalline monohydrate	15 mg/mL	22	16	5	>50	>50	No	<2, <2, <1

Preclinical Species PK Profiles

Wistar Han Rat PK Profile					Beagle Dog PK Profile					C57BL/6 Mouse PK Profile					Human
Cl / Cl_{int} (mL/min/kg)	V_d / V_{du} (L/kg)	$t_{1/2}$ (h)	F (%)	PPB (%)	Cl / Cl_{int} (mL/min/kg)	V_d / V_{du} (L/kg)	$t_{1/2}$ (h)	F (%)	PPB (%)	Cl / Cl_{int} (mL/min/kg)	V_d / V_{du} (L/kg)	$t_{1/2}$ (h)	F (%)	PPB (%)	PPB (%)
8.1 / 64[c]	1.0 / 6.3	2.7	55	82	4.3 / 6.2[d]	1.5 / 1.8	4.7	95	10	4.5 / 10[e]	0.2 / 0.4	0.8	77	53	30

Figure 3. Potency, PK profile, and crystal structure of **3c** (MSD-496486311) with PI3K*δ* (2.8 Å). PDB ID: 7LM2. [a]LLC-PK1 cell line; [b]MDCKII cell line; [c]0.5 mg/kg *iv*, 1 mg/kg *po*; [d]0.25 mg/kg *iv*, 0.5 mg/kg *po* in saline (*iv*) or 0.5% methyl cellulose (*po*); [e]1 mg/kg *iv*, 3 mg/kg *po* in DMSO/PEG400/H_2O-20/60/20; n = 3.

and 69% in rats and dogs). Consequently, human dose predictions for optimized ureas were inferior (180 mg *qd* with a P/T of 27 for optimized urea **3k**).

With the success of methyl ether-substituted cyclobutyl amides **3g** and **3h**, we explored the larger cyclic ethers **3m**, **3n**, **3o**, and **3p**. For tetrahydrofuran amides **3m** and **3n**, the potency was maintained versus **3g** and **3h**, and plasma intrinsic clearances were low; however, the half-lives were suboptimal ($t_{1/2}$ = 1.4 and 3.8 in rats and dogs for **3n**) due to lower unbound volumes in both species than the methoxycyclobutyl amides. This lower V_{du} is consistent with lower HPLC Log *D* values (0.3 units lower than **3g** and **3h**). To close the loop with starting point **1**, we prepared the tetrahydropyran amides as well; however, we noted inferior potency and short half-lives. This was not a surprise given the results of the bile duct cannulation with **1**, indicating metabolism of the tetrahydropyran ring. In addition to alkyl and cycloalkyl amides, we also explored a variety of aromatic amides. Generally few aromatic amides could match the potency achieved with small cycloalkyl amides, with one somewhat successful example being 4-oxazole amides **3q** and **3r**. Biochemical potency was good for both, and half-lives for **3r** in particular were reasonable ($t_{1/2}$ = 1.7 and 1.8 h for rats and dogs); however, dose predictions were not competitive since the human whole blood potency was inferior.

As part of the optimization process to identify additional inhibitors to mitigate any potential issues that we may encounter later in development, we cross-checked our best amide and urea pyrrolidine capping groups with several purine C(8) aromatic groups identified earlier in the campaign. Shown in Table 3 is the SAR generated for one such series, the 6-trifluoromethylpyridine substituent at purine C(8). As a whole, the trifluoromethyl pyridine series was as potent as the methylpyrimidine series summarized in Table 2 but was significantly less polar with the cLogP and HPLC Log *D* values about 1 unit greater in head-to-head comparisons. At the outset, we hoped that this physical property space would render inhibitors with a higher unbound volume of distribution and consequently more optimizable to longer rat and dog half-lives. In fact, the trifluoromethyl pyridines bearing the cyclopropyl amide, **4a** and **4b**, did have larger unbound volumes (e.g., V_{du} = 8.8, 3.9 L/kg for **4a**); however, they also had higher plasma clearances, and so half-lives of only 0.7−1.2 h were achieved. Furthermore, NH-linked analogs prepared in this series were potent inhibitors of adenosine uptake in HeLa cells. For example, compound **4a** inhibited adenosine uptake in HeLa cells with an IC_{50} of 1.2 μM. This was consistent with our previous observation that increased lipophilicity often led to adenosine uptake activity, especially for NH-linked pyrrolidines. For this reason, we continued optimization in this subseries with O-linked pyrrolidines only.

To rebalance the polarity and lower lipophilicity, we again turned to ether-containing amides. *cis*-3-Methoxycyclobutyl amide **4c** did have significantly improved PK, with promising half-lives (3.3, 2.6 h) that were consistent with the higher unbound volumes (13, 2.5 L/kg) as well as good bioavailability (39, 100%) in rats and dogs. 3-Methoxyazetidine urea **4d** had lower unbound volume of distribution in both rats and dogs and shorter half-lives in both species ($t_{1/2}$ = 2.0 and 0.7 h in rats and dogs), as observed for the 2-methylpyrimidine series in Table 2. Hence, while the human dose prediction for **4c** was promising (90 mg *qd* with P/T = 10), the prediction for the urea **4d** was not (130 mg *qd* with P/T = 43) owing to a shorter predicted half-life in human for **4d**. It was the tetrahydrofuran and oxazole amides **4e** and **4f** that offered the best PK in the trifluoromethyl pyridine series. They were polar amides within

https://doi.org/10.1021/acs.jmedchem.1c00237
J. Med. Chem. 2021, 64, 5137−5156

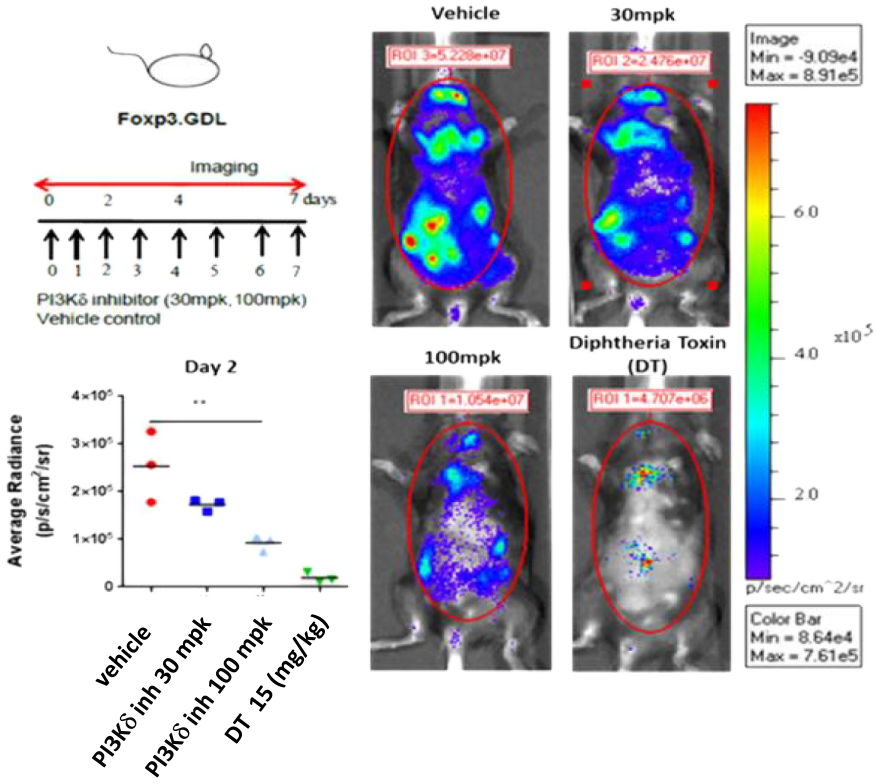

Figure 4. Reduction of regulatory T (Treg) cells in Foxp3-GDL reporter mice following treatment with **3c** at 30 and 100 mg/kg. Diphtheria toxin (DT) was used as a control. Radiance is expressed as photons/s/cm^2/steradian.

the 2-methylpyrimidine series, having lower HPLC Log *D* values and unbound volumes; however, they were optimal when combined with the 2-trifluoromethylpyridine moiety. Plasma intrinsic clearances were low for **4e** and **4f**, and this resulted in excellent half-lives for both **4e** ($t_{1/2}$ = 2.3 and 3.6 h in rats and dogs) and **4f** ($t_{1/2}$ = 6.0 and 2.5 h in rats and dogs) with excellent bioavailability. The unbound volumes for **4e** and **4f** were comparable to optimized analogs in the 2-methylpyrimidine series, indicating that we had optimized to a similar overall physical property space and were again unable to achieve longer half-lives using an unbound volume strategy. These PK profiles supported low predicted human doses of 8 and 20 mg *qd* for **4e** and **4f**, respectively, with a low P/T = 4 for both.

With the promising preliminary potency and PK profiles of **3c**, we completed characterization of this inhibitor, shown in Figure 3. A crystal structure of **3c** bound to PI3Kδ confirmed a binding mode very similar to what was observed for **1**; the purine makes hydrogen bond contacts to the kinase hinge region while the pyrrolidine amide gears the cyclopropane toward Trp760 residue. Lead compound **3c** has excellent potency in the Ramos Burkitt's lymphoma-derived B cell line (AKT pSer473 IC_{50} 20 nM) and in human whole blood (B-cell activation biomarker CD69 IC_{50} = 65 nM, basophil activation biomarker CD63 IC_{50} = 50 nM). The enzyme potency was maintained from humans to mice, rats, and dogs, as expected. Lead **3c** was then evaluated in numerous in vitro safety panels. In a 280-kinase panel at Invitogen (Thermo Fisher Scientific), no kinase activity was found within 100× of the PI3Kδ IC_{50} value of 1.6 nM. The closest identified off-targets were PI3Kα (150× selectivity), PI3Kβ (1370×), and PI3Kγ (3690×). No activity was identified in the Eurofins Panlabs safety pharmacology panel of 116 receptors and enzymes at 10 μM. Compound **3c** was not an inhibitor of potassium hERG, sodium Nav1.5, or calcium Cav1.2 ion channels (IC_{50} > 50 μM). It was not an inhibitor of major CYP enzymes, CYP-1A2, 2B6, 2C8, 2C9, 2C19, 2D6, and 3A4 (IC_{50} > 50 μM); hence, it is unlikely to be a perpetrator of CYP-mediated DDI. Furthermore, no significant induction response was observed for CYP-3A4, 2B6, and 1A2, suggesting low potential for DDI. Lastly, **3c** was not a time-dependent inhibitor of CYP-3A4.

Compound **3c** was stable when incubated in hepatocytes across all species (Cl_{int} < 2 mL/min/kg, rats, dogs, monkeys, humans). Renal clearance was expected to be the major route of elimination in humans given the stability to hepatocytes as well as the observed routes of elimination in rats and dogs. In bile duct cannulated (BDC) studies in rats and dogs dosed with [2-^{3}H-purine]-**3c**, the majority of the radioactivity was excreted in urine as the unchanged parent compound. More specifically, 75% of the recovered radioactivity in excreta following *iv* dose in rats was the unchanged parent with renal excretion as the major clearance mechanism (Cl_{renal} 2× GFR; indicating active secretion). Following a *po* dose in dogs, 65% of the recovered radioactivity was the unchanged parent as renal and biliary excretion (Cl_{renal} = GFR; indicating passive filtration). The balance of radioactivity in rat and dog BDC studies was eliminated in bile and urine as oxidative metabolites and numerous pyrrolidine products. Consistent with these observations, the compound had good permeability in the LLC-PK1 assay (Papp of 22 × 10^{-6} cm/s), with transport observed in the MDCKII transport assay expressing MDR1 PGP (BA/AB 16); however, **3c** was not an inhibitor of PGP (IC_{50} > 300 μM). In addition, **3c** was not an inhibitor of OATP1B1.

Compound **3c** was isolated as a stable non-hygroscopic crystalline monohydrate with good solubility in simulated

https://doi.org/10.1021/acs.jmedchem.1c00237
J. Med. Chem. 2021, 64, 5137−5156

intestinal fluid (14 mg/mL) and neutral water (15 mg/mL). It has a pK_a of 3.06 with protonation on the purine ring, moderate MW (392.47 g/mol), HPLC Log *D* (0.8), and PSA (105 Å). The solubility in the preclinical formulation of 0.5% methocel was 150 mg/mL.

IN VIVO PHARMACOLOGY

Lead compound **3c** (MSD-496486311) was evaluated in rodent models to corroborate potency in B-cell and basophil activation whole blood assays. Two models described here are the Foxp3-GFP mouse model to monitor the population and localization of regulatory T cells and the Brown Norway rat ovalbumin model for allergic rhinitis and asthma PK/PD readouts.

Tumor-induced immunosuppression constitutes a significant obstacle for effective cancer immunotherapy. Regulatory T (Treg) cells play key roles in the maintenance of immune homeostasis, and expression of the transcription factor forkhead box P3 (Foxp3) is a widely used Treg marker.[15] Cancer patients have elevated numbers of Treg cells within the blood and lymphoid tissues as well as the tumor microenvironment. For some patients, increased Treg populations correlate with a poor prognosis, and Tregs have been proposed to aid tumors in evading immune surveillance. In vitro studies indicate that PI3K/AKT signaling is required for Tregs to mature and suppress anticancer immune responses,[15] and inhibitors of PI3Kδ have been shown to impair the immunosuppressive function of Tregs in mice while leaving cytotoxic T cell responses intact.[16−18] To confirm the impact of PI3Kδ inhibition on regulatory T cell proliferation and localization in mice with our inhibitor, we used the C57BL/6-Foxp3 reporter mouse model available from Jackson Laboratory.[19] These Foxp3-GFP mice co-express GFP (green fluorescent protein) and the regulatory T cell-specific transcription factor Foxp3, such that GFP expression accurately identifies the Foxp3+ T cell population.

Foxp3-GFP mice were treated for up to 7 days with PI3Kδ inhibitor **3c** at 30 and 100 mg/kg/day. Bioluminescence imaging was performed 10 min following *ip* injection of 3 mg of luciferin using an IVIS Spectrum imaging system, and radiance was quantified in units of photons/s/cm^2/steradian. Diphtheria Toxin (DT) was used as a positive control, as DT is cytotoxic and completely ablates Treg. Consistent with the literature, a dose-dependent decrease of Treg population was observed in mice upon treatment with **3c** (Figure 4). Interestingly, a plateau of 70% Treg reduction was observed with **3c**, unlike DT, which also induces spontaneous autoimmunity. Hence, PI3Kδ inhibition might be a safer modulator of Treg cells. The exposure for **3c** in mice when dosed at 100 mpk was AUC = 133 μM h, C_{max} = 33 μM, and C_{trough} = 110 nM. This equated to an unbound uC_{max} = 16 μM and an unbound uC_{trough} = 52 nM. The unbound uC_{trough} level in mice required to achieve 70% Treg reduction is comparable to the human whole blood CD69 unbound uIC_{50} value of 47 nM. Note that these studies were performed in accordance to the guidelines of the Institute for Laboratory Animal Research (LAR). All studies were part of an institutional animal care and use committee (IACUC)-approved protocol and animals were housed in an AAALAC international accredited research facility.

In addition to monitoring the impact of PI3Kδ inhibition on the B-cell surface biomarker CD69 in whole blood, we monitored PI3Kδ inhibitor-mediated inhibition of the upregulation of basophil degranulation CD63 surface biomarker following anti-IgE activation. The CD63 biomarker is more relevant for the treatment of respiratory diseases predominately mediated by type 2 T helper (TH2) cells. For compound **3c**, the human whole blood CD63 inhibition potency was IC_{50} = 50 nM (unbound uIC_{50} = 36 nM), consistent with the inhibition of CD69 surface biomarker upregulation by anti-CD76b. We used the Brown Norway rat model for allergic rhinitis and asthma, and results with **3c** was published in greater detail elsewhere[20] (where **3c** was identified as MSD-496486311). Rats were presensitized for 14 days by daily treatment with ovalbumin (0.020 mg *ip*). These rats were then administered with **3c** (0.3−30 mg/kg *po*) for 2 days, and then after 1 h following the second dose, they were treated with ovalbumin. After 48 h, the BAL (pulmonary bronchoalveolar lavage) inflammation eosinophil cell count was assessed. The data is shown in Figure 5. The 10 mg/kg dose with C_{trough} = 14 nM (unbound = 8 nM given Brown Norway rat PPB 41%) approximates a 50% reduction in the BAL count, while a 30 mg/kg dose with C_{trough} = 103 nM (unbound 62 nM) elicits a full response by BAL count. This potency is consistent with what we observed in the human CD63 whole blood assay.

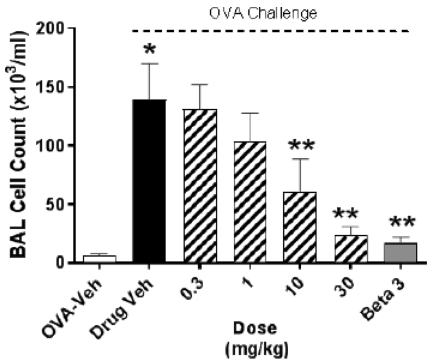

Figure 5. Attenuation of allergic-mediated pulmonary inflammation in ovalbumin-sensitized and challenged Brown Norway rat by treatment with **3c**.

SYNTHESIS

The 9-alkyl-8-aryl-6-chloropurine precursors used to access new inhibitors were prepared via the routes outlined in Scheme 1: either through condensation of arylaldehydes with a diaminopyrimidine or through a Suzuki coupling with 9-alkyl-8-iodopurines. For example, *N*-ethyl-1*H*-5-methyl-pyrazole-4-carboxaldehyde **I** was condensed under oxidative conditions with $FeCl_3$ and air to 6-chloro-N4-methylpyrimidine-4,5-diamine **II**, giving 6-chloro-8-(1-ethyl-5-methyl-1*H*-pyrazol-4-yl)-9-methyl-9*H*-purine (**III**). Alternatively, 6-chloropurine was selectively alkylated at N(9) with K_2CO_3 and ethyl iodide and then iodinated at C(8) with LDA and I_2 giving **VII**. Suzuki coupling with 2-methylpyrimidine-5-boronic ester gave 6-chloro-9-ethyl-8-(2-methylpyrimidin-5-yl)-9*H*-purine (**X**).

Hydroxypyrrolidine inhibitors containing ether linkers were prepared by treatment of a chloropurine precursor from Scheme 1 with an alcohol and NaH. Aminopyrrolidines were prepared from the corresponding primary amine with iPr_2NEt or K_2CO_3 at 80 °C (Scheme 2). In some cases, a selectivity motif was introduced bearing a protective group (e.g., an *N*-

https://doi.org/10.1021/acs.jmedchem.1c00237
J. Med. Chem. 2021, 64, 5137−5156

Scheme 1. Synthesis of Chloropurine Precursors[a]

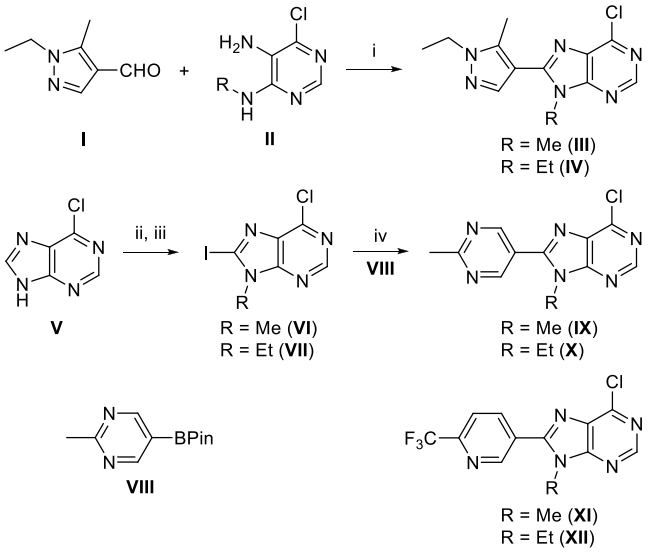

[a]Reagents and conditions: (i) $FeCl_3·6H_2O$, air, DMF, 85 °C, 75−88%; (ii) EtI, K_2CO_3, DMSO, 53%; (iii) LDA, I_2, THF, −78 °C, 62%; (iv) Pd(dppf)Cl_2·DCM, K_2CO_3, dioxane, water, 90 °C, 56%.

Scheme 2. General assembly of amino- and hydroxypyrrolidine purines from chloropurine intermediates[a]

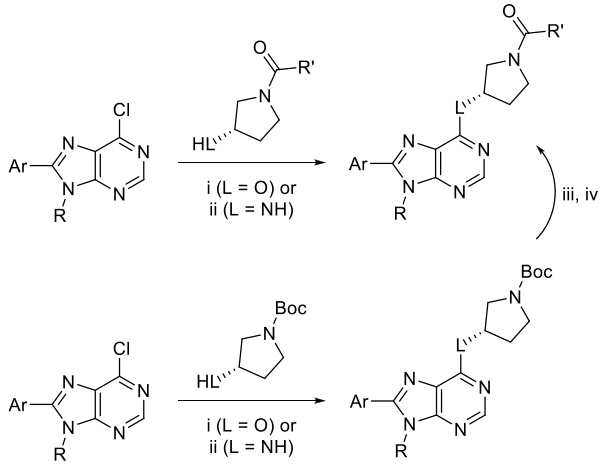

[a]Reagents and conditions: (i) NaH, THF, 0 °C to RT; (ii) iPr_2NEt or K_2CO_3, DMF or t-BuOH, 80 °C; (iii) TFA, DCM or HCl, dioxane; (iv) RCOCl, iPr_2NEt, DMF or RCO_2H, HATU, DMF.

Boc group), then after the nucleophilic displacement step, the protective group was removed using standard conditions (e.g., TFA or HCl) and the pyrrolidine was capped (e.g., amide formation with acid chloride or acid and HATU). Specific synthetic details are available in the Experimental Section for all compounds.

CONCLUSIONS

In summary, beginning with pyrrolidine **1**, we learned that growing from an N-Me-purine core to an N-Et-purine core gave an 8× boost in potency by filling the hydrophobic cavity below gatekeeper residue Ile825 and above Tyr813 that is unique to lipid kinases. We next learned that replacing the *N*-ethyl-pyrazole ring with a 2-methylpyrimidine ring improved the metabolic stability and half-life in preclinical species. The gearing effect of the (*S*)-pyrrolidine amide toward Trp is critical for kinome and isoform selectivity, with small amides adequate and preferred for excellent selectivity. Optimization gave N-linked compound **3c** representing a structurally distinct PI3Kδ inhibitor with excellent potency in whole blood and selectivity over the PI3K family. Taken together with good half-lives in preclinical species and solubility, inhibitor **3c** is predicted to have a low once-daily predicted human dose of 35 mg *qd* to maintain CD69 IC_{50} coverage, or 76 mg *bid*, to maintain an IC_{90} coverage, with a dose number of <1. With the low volume of distribution generally observed in the purine pyrrolidine series, we resorted to driving intrinsic clearance as low and potency as high as possible to achieve acceptable predicted human doses. Concurrent with the characterization of **3c**, we identified several additional inhibitors with low predicted human dose, such as N- and O-linked 3-methoxycyclobuyl amides **3g** and **3h**. Reoptimization with the trifluoromethylpyridine purine substituent led to O-linked **4e** and **4f** bearing tetrahydrofuran and oxazole amides to introduce greater structural diversity in our portfolio of pyrrolidine PI3Kδ inhibitors. While lowering intrinsic clearance was the more successful strategy, small boosts in unbound volume also contributed to increasing the half-life and lowering the projected human doses. Compound **3c** (MSD-496486311) offers a distinct structure from currently approved PI3Kδ inhibitors for the treatment of hematologic malignancies driven by the AKT pathway.

EXPERIMENTAL SECTION

General Synthetic Chemistry Methods. Reactions were performed in dried round-bottom flasks or capped vials with stirring under an inert atmosphere of nitrogen unless stated otherwise. Solvents in septum-sealed bottles and reagents were obtained from commercial suppliers and used as received. All temperatures are in degrees Celsius (°C), and ambient temperature is 20 °C. Microwave reactions were performed with a Biotage Initiator Series microwave. Most compounds were purified by reverse-phase preparative HPLC or MPLC on silica gel. The course of the reactions was followed by LC/MS (30 mm × 2 mm, 2 μm column; 3 to 98% MeCN/water with 0.05% TFA gradient over 2.3 min; 0.9 mL/min flow rate; ESI; UV detection at 254 nm). Products were analyzed by NMR, LC/MS, and HRMS. NMR spectra were recorded on either a 400, 500, or 600 MHz Varian spectrometer, chemical shifts are reported in parts per million (ppm) relative to tetramethylsilane and referenced to residual solvent. Coupling constants are reported in Hz. HRMS was obtained with a Waters Acquity UPLC coupled to a Waters Xevo G2 QTof using ESI+ detection. The purity of all compounds screened in the biological assays was examined by LC/MS analysis (100 mm × 3 mm C18 column; 3 to 98% MeCN/water with 0.05% TFA gradient over 5 min run; UV detection at 215 nm) and was found to be ≥95%.

6-Chloro-8-(1-ethyl-5-methyl-1H-pyrazol-4-yl)-9-methyl-9H-purine (III). A 1000 mL three-neck flask fitted with a thermometer was charged with *N*-ethyl-1*H*-5-methyl-pyrazole-4-carboxaldehyde (**I**, 68.5 g, 496 mmol), anhydrous *N*,*N*-dimethylformamide (400 mL), and 6-chloro-*N*-methylpyrimidine-4,5-diamine (**II**, 71.5 g, 451 mmol). The reaction mixture was stirred at RT for 10 min to ensure dissolution of all solid materials. Iron(III) chloride hexahydrate (122 g, 451 mmol) was then added over the course of 5 min, resulting in the formation of a dark brown solution. A stream of air was continuously bubbled through the stirred reaction mixture, which was heated to 85 °C and stirred for 14 h. The mixture was poured into 2500 mL of crushed ice and water, and the resulting pale orange precipitate was collected by vacuum filtration and dried on the filter. The solid was triturated with ethanol (500 mL) at 50 °C for 2 h and at RT overnight. The residue was collected by vacuum filtration and dried on the filter to give 93.5 g

https://doi.org/10.1021/acs.jmedchem.1c00237
J. Med. Chem. 2021, 64, 5137−5156

(75% yield) of intermediate 6-chloro-8-(1-ethyl-5-methyl-1*H*-pyrazol-4-yl)-9-methyl-9*H*-purine (**III**) as a pale yellow solid. ^{1}H NMR (400 MHz, DMSO-d_6) δ 8.67 (s, 1 H), 8.09 (s 1 H), 4.18 (q, 2 H), 3.89 (s, 3 H), 2.63 (s, 3 H), 1.35 (t, 3 H); MS (EI) calcd for $C_{12}H_{14}ClN_6$ $[M + H]^+$, 277; found 277.

6-Chloro-9-ethyl-8-(1-ethyl-5-methyl-1H-pyrazol-4-yl)-9H-purine (IV). Intermediate **IV** was prepared following a synthetic sequence analogous to that used for the synthesis of **III**, obtaining 88% yield of **IV**. ^{1}H NMR (600 MHz, $CDCl_3$) δ 8.65 (s, 1 H), 7.75 (s, 1 H), 4.42 (q, 2 H), 4.20 (q, 2 H), 2.62 (s, 3 H), 1.50 (t, 3 H), 1.45 (t, 3 H); MS (EI) calcd for $C_{13}H_{16}ClN_6$ $[M + H]^+$, 291; found 291.

6-Chloro-9-ethyl-8-iodo-9H-purine (VII). Into a 10 L four-neck round-bottom flask was placed a solution of 6-chloro-9*H*-purine (400 g, 2.59 mol), iodoethane (405 g, 2.60 mol), and potassium carbonate (430 g, 3.11 mol) in DMSO (4 L). The resulting solution was stirred overnight at RT, diluted with ice water, and extracted with MTBE. The organic extracts were combined, dried ($MgSO_4$), and concentrated under vacuum. The residue was purified by chromatography on SiO_2 (1:10 to 1:1 EtOAc/petroleum ether) providing 250 g (53%) of 6-chloro-9-ethyl-9*H*-purine. Into a 10 L four-neck round-bottom flask purged and maintained with an inert atmosphere of nitrogen was placed a solution of diisopropylamine (200 g, 1.98 mol) in THF (1.2 L). This was followed by addition of a 2.5 M solution of *n*-BuLi (736 mL, 1.40 equiv) at −78 °C. After stirring for 30 min, a solution of 6-chloro-9-ethyl-9*H*-purine (240 g, 1.31 mol) in THF (1.2 L) was added dropwise with stirring at −78 °C. The solution was stirred for 5 min at −78 °C, followed by addition of a solution of I_2 (467 g, 1.84 mol) in THF (1.2 L) at −78 °C. The solution was stirred for an additional 10 min at −78 °C and then quenched by the addition of 200 mL of aqueous NH_4Cl. The organic layer was washed with aqueous $Na_2S_2O_3$, dried ($MgSO_4$), and concentrated under vacuum. The solid was washed with 2 × 200 mL of ethyl ether to give 250 g (62%) 6-chloro-9-ethyl-8-iodo-9*H*-purine (**VII**). ^{1}H NMR (400 MHz, DMSO-d_6) δ 8.73 (s, 1 H), 4.28 (q, J = 7.2 Hz, 2 H), 1.37 (t, J = 7.2 Hz, 3 H); MS (EI) calcd for $C_7H_7N_4ClI$ $[M + H]^+$, 309; found, 309.

6-Chloro-9-methyl-8-(2-methylpyrimidin-5-yl)-9H-purine (IX). Intermediate **IX** was prepared following a synthetic sequence analogous to that used for the synthesis of **X**, obtaining 68% yield of **IX**. ^{1}H NMR (300 MHz, $CDCl_3$) δ 9.18 (s, 2 H), 8.88 (s, 1 H), 3.97 (s, 3 H), 2.89 (s, 3 H); MS (EI) calcd for $C_{11}H_{10}ClN_6$ $[M + H]^+$, 261; found, 261.

6-Chloro-9-ethyl-8-(2-methylpyrimidin-5-yl)-9H-purine (X). Into a 5 L four-neck round-bottom flask purged and maintained with an inert atmosphere of nitrogen was placed a solution of 6-chloro-9-ethyl-8-iodo-9*H*-purine (200 g, 648 mmol), 2-methyl-5-(4,4,5,5-tetramethyl-1,3,2-dioxaborolan-2-yl)pyrimidine (180 g, 818 mmol), potassium carbonate (134 g, 970 mmol), and Pd(dppf)Cl_2-DCM (30 g, 39 mmol) in dioxane (2.0 L) and water (400 mL). The resulting solution was stirred for 6 h at 90 °C. The reaction mixture was cooled to RT, diluted with water, and then extracted with EtOAc. The organic extracts were combined, dried ($MgSO_4$), and concentrated under vacuum. The residue was purified by chromatography on SiO_2 (1:1:1 petroleum ether/DCM/EtOAc) providing 100 g (56%) of 6-chloro-9-ethyl-8-(2-methylpyrimidin-5-yl)-9*H*-purine (**X**). ^{1}H NMR (300 MHz, $CDCl_3$) δ 9.12 (s, 2 H), 8.80 (s, 1 H), 4.49 (q, J = 7.2 Hz, 2 H), 2.89 (s, 3 H), 1.51−1.57 (t, J = 7.2 Hz, 3 H). MS (EI) calcd for $C_{12}H_{12}N_6Cl$ $[M + H]^+$, 275; found, 275.

Chloro-9-methyl-8-(6-(trifluoromethyl)pyridin-3-yl)-9H-purine (XI). A solution of 6-chloro-N4-methylpyrimidine-4,5-diamine (300 mg, 1.89 mmol) in DMF (1 mL) was treated with iron(III) chloride hexahydrate (204 mg, 0.756 mmol), followed by 6-(trifluoromethyl)-nicotinaldehyde (364 mg, 2.08 mmol). The reaction mixture was heated at 85 °C with air bubbling through the reaction mixture for 48 h. Next, the mixture was cooled to RT and water was added. The mixture was extracted with DCM, dried (Na_2SO_4), filtered, and concentrated. The residue was purified by chromatography on SiO_2 (MeOH/DCM; 1/60 to 1/40) to give 6-chloro-9-methyl-8-(6-(trifluoromethyl)pyridin-3-yl)-9*H*-purine as a white solid. ^{1}H NMR (400 MHz, $CDCl_3$) δ 9.25 (s, 1 H), 8.85 (s, 1 H), 8.49−8.51 (m, 1 H), 7.95−7.97 (m, 1 H), 4.09 (s, 3 H); MS (EI) calcd for $C_{12}H_8ClF_3N_5$ $[M + H]^+$, 314; found, 314.

6-Chloro-9-ethyl-8-(6-(trifluoromethyl)pyridin-3-yl)-9H-purine (XII). A solution of 6-chloro-9-ethyl-8-iodo-9*H*-purine (3.0 g, 9.7 mmol) in dioxane (40 mL) and water (4 mL) was treated with K_2CO_3 (4.0 g, 29 mmol), Pd(dppf)Cl_2 (1.1 g, 1.5 mmol), and (6-(trifluoromethyl)pyridin-3-yl)boronic acid (2.0 g, 11 mmol). The mixture was stirred for 12 h at 90 °C, then quenched by the addition of water (50 mL), and extracted with DCM (3 × 100 mL). The organic layers were combined, dried ($MgSO_4$), and filtered. The filtrate was concentrated and purified by chromatography on SiO_2 (10% EtOAc/petroleum ether) to afford 6-chloro-9-ethyl-8-(6-(trifluoromethyl)pyridin-3-yl)-9*H*-purine (1.2 g, 3.7 mmol, 38% yield) as a white solid. ^{1}H NMR (300 MHz, DMSO-d_6) δ 9.26 (s, 1 H), 8.89 (s, 1 H), 8.62 (m, 1 H), 8.20 (m, 1 H), 4.50 (m, 2 H), 1.40 (m, 3 H); MS (EI) calcd for $C_{13}H_{10}ClF_3N_5$ $[M + H]^+$, 328; found, 328.

(S)-(3-((8-(1-Ethyl-5-methyl-1H-pyrazol-4-yl)-9-methyl-9H-purin-6-yl)oxy)pyrrolidin-1-yl)(tetrahydro-2H-pyran-4-yl)methanone (1). A solution of (*S*)-pyrrolidin-3-ol (15.0 g, 172 mmol) and triethylamine (19.2 g, 189 mmol) in 100 mL of DCM was treated dropwise at 0 °C with a solution of tetrahydro-2*H*-pyran-4-carbonyl chloride (26.4 g, 177 mmol) in 75 mL of DCM. The mixture was stirred for 2 h and concentrated. The residue was taken up in 1 L of EtOAc, stirred overnight, and then filtered to remove amine salts. The mother liquor was concentrated to provide 36 g (100%) of (*S*)-(3-hydroxypyrrolidin-1-yl)(tetrahydro-2*H*-pyran-4-yl)methanone. ^{1}H NMR (600 MHz, $CDCl_3$) δ 4.52 (d, J = 6.0 Hz, 1 H), 3.99−4.03 (m, 2 H), 3.38−3.70 (m, 6 H), 2.50−2.64 (m, 1 H), 1.98−2.06 (m, 2 H), 1.86−1.93 (m, 2 H), 1.60−1.71 (m, 2 H). A solution of (*S*)-(3-hydroxypyrrolidin-1-yl)(tetrahydro-2*H*-pyran-4-yl)methanone (4.32 g, 21.7 mmol) in 60 mL of THF was treated at 0 °C with a 60% mineral oil suspension of sodium hydride (1.01 g, 25.2 mmol) followed by 6-chloro-8-(1-ethyl-5-methyl-1*H*-pyrazol-4-yl)-9-methyl-9*H*-purine (Intermediate **III**, 5.00 g, 18.1 mmol). The reaction mixture was stirred for 2 h and allowed to warm to RT. The crude reaction mixture was concentrated, and the residue was purified by chromatography on SiO_2 (gradient of 0−20% MeOH/DCM) to give 5.0 g (63%) of **1**. $[\alpha]_D$ = +29° (c 0.58, $CHCl_3$); ^{1}H NMR (600 MHz, $CDCl_3$) δ 8.48 (d, J = 7.0 Hz, 1 H), 7.75 (d, J = 6.3 Hz, 1 H), 5.93 (s, 1 H), 4.16−4.20 (m, 2 H), 3.93−4.04 (m, 3 H), 3.87, 3.89 (2 s, 3 H), 3.70−3.86 (m, 3 H), 3.35−3.45 (m, 2 H), 2.52−2.65 (m, 1 H), 2.56, 2.60 (2 s, 3 H), 2.45−2.50 (m, 1 H), 2.23−2.40 (m, 2 H), 1.86−1.94 (m, 2 H), 1.60−1.66 (m, 2 H), 1.45 (t, J = 6 Hz, 3 H); ^{13}C NMR (125 MHz, DMSO-d_6) δ 172.9, 158.6, 154.2, 150.9, 148.6, 139.9, 138.0, 120.8, 108.7, 76.7, 75.2, 66.7, 52.0, 44.1, 39.0, 38.9, 31.9, 30.7, 30.1, 28.8, 15.4, 10.6; HRMS (EI) calcd for $C_{22}H_{30}N_7O_3$ $[M + H]^+$, 440.2410; found, 440.2414.

(S)-1-(3-(8-(1-Ethyl-5-methyl-1H-pyrazol-4-yl)-9H-purin-6-ylamino)pyrrolidin-1-yl)propan-1-one (2a). Prepared in a fashion similar to that used for the synthesis of **2b**, in which precursor 6-chloro-N4-methylpyrimidine-4,5-diamine is replaced by 6-chloropyrimidine-4,5-diamine. ^{1}H NMR (500 MHz, DMSO-d_6) δ 8.18 (br, 1 H), 8.00 (s, 1 H), 7.56 (br m, 1 H), 4.78 (m, 1 H), 4.14 (q, J = 7.2 Hz, 2 H), 3.82 (m, 1 H), 3.63−3.74 (m, 1 H), 3.55 (m, 1 H), 3.46 (m, 1 H), 3.38 (m, 1 H), 2.72 (s, 3 H), 2.21−2.31 (m, 2 H), 1.99−2.18 (m, 2 H), 1.34 (t, J = 7.2 Hz, 3 H), 0.99 (m, 3 H); HRMS (EI) calcd for $C_{18}H_{25}N_8O$ $[M + H]^+$, 369.2151; found, 369.2152.

(S)-1-(3-((8-(1-Ethyl-5-methyl-1H-pyrazol-4-yl)-9-methyl-9H-purin-6-yl)amino)pyrrolidin-1-yl)propan-1-one (2b). A solution of 6-chloro-8-(1-ethyl-5-methyl-1*H*-pyrazol-4-yl)-9-methyl-9*H*-purine (**III**, 500 mg, 1.81 mmol) in DMF (18 mL) was treated with iPr_2NEt (0.80 mL, 4.6 mmol) and (*S*)-*tert*-butyl-3-aminopyrrolidine-1-carboxylate (0.55 mL, 3.1 mmol). The mixture was stirred at 80 °C for 72 h. The mixture was diluted with EtOAc, washed with water and brine, dried (Na_2SO_4), and concentrated. The residue was purified by chromatography on SiO_2 (gradient of 0−10% MeOH/DCM) to afford (*S*)-*tert*-butyl-3-((8-(1-ethyl-5-methyl-1*H*-pyrazol-4-yl)-9-methyl-9*H*-purin-6-yl)amino)pyrrolidine-1-carboxylate (345 mg, 45%). ^{1}H NMR (600 MHz, DMSO-d_6) δ 8.19 (s, 1 H), 7.89 (s, 1

https://doi.org/10.1021/acs.jmedchem.1c00237
J. Med. Chem. 2021, 64, 5137−5156

H), 7.73 (s, 1 H), 4.13 (q, J = 7.2 Hz, 2 H), 3.72 (s, 3 H), 3.54−3.65 (m, 1 H), 3.40−3.50 (m, 1 H), 3.18−3.35 (m, 3 H), 2.52 (s, 3 H), 2.05−2.20 (m, 1 H), 1.90−2.04 (m, 1 H), 1.33−1.38 (2s, 9 H), 1.32 (t, J = 7.3 Hz, 3 H); MS (EI) calcd for $C_{21}H_{31}N_8O_2$ $[M + H]^+$, 427; found 427.

A solution of (*S*)-*tert*-butyl-3-((8-(1-ethyl-5-methyl-1*H*-pyrazol-4-yl)-9-methyl-9*H*-purin-6-yl)amino)pyrrolidine-1-carboxylate (345 mg, 0.809 mmol) in dioxane (2 mL) was treated with 4 M HCl in dioxane (1 mL, 4 mmol). The mixture was stirred at RT for 2 days and concentrated giving (*S*)-8-(1-ethyl-5-methyl-1*H*-pyrazol-4-yl)-9-methyl-*N*-(pyrrolidin-3-yl)-9*H*-purin-6-amine, HCl (323 mg, 100% yield). MS (EI) calcd for $C_{16}H_{23}N_8$ $[M + H]^+$, 327; found 327.

A solution of (*S*)-8-(1-ethyl-5-methyl-1*H*-pyrazol-4-yl)-9-methyl-*N*-(pyrrolidin-3-yl)-9*H*-purin-6-amine, HCl (20 mg, 0.046 mmol) in DMF (0.5 mL) was treated with propionyl chloride (5 μL, 0.06 mmol) and TEA (0.05 mL, 0.36 mmol). The mixture was stirred at RT for 16 h, filtered, and purified by reverse-phase chromatography (gradient of water/MeCN with 0.1% TFA) to afford (*S*)-1-(3-((8-(1-ethyl-5-methyl-1*H*-pyrazol-4-yl)-9-methyl-9*H*-purin-6-yl)amino)-pyrrolidin-1-yl)propan-1-one (21 mg, 90% yield). ^{1}H NMR (600 MHz, DMSO-d_6) δ 8.32 (s, 1 H), 7.93 (s, 1 H), 4.14 (q, J = 7.2 Hz, 2 H), 3.76 (s, 3 H), 3.64−3.70 (m, 1 H), 3.56−3.64 (m, 1 H), 3.44−3.54 (m, 2 H), 3.30−3.42 (m, 1 H), 2.52 (s, 3 H), 1.95−2.30 (m, 4 H), 1.32 (t, J = 7.2 Hz, 3 H), 0.94 (t, J = 7.4 Hz, 3 H); HRMS (EI) calcd for $C_{19}H_{27}N_8O$ $[M + H]^+$, 383.2308; found 383.2309.

*9-Ethyl-8-(1-ethyl-5-methyl-1H-pyrazol-4-yl)-N-[(3S)-1-propanoylpyrrolidin-3-yl]-9H-purin-6-amine (**2c**).* Prepared in a fashion similar to that used for the synthesis of **2b**, in which precursor intermediate **III** is replaced by intermediate **IV**; 6-chloro-9-ethyl-8-(1-ethyl-5-methyl-1*H*-pyrazol-4-yl)-9*H*-purine. $[\alpha]_D$ = +22° (c 0.5, MeOH); ^{1}H NMR (600 MHz, DMSO-d_6) δ 8.24 (br, 1 H), 7.87 (br, 1 H), 7.83 (br, 1 H), 4.78 (br, 1 H), 4.22 (br, 2 H), 4.18 (q, J = 6 Hz, 2 H), 3.81 (m, 1 H), 3.63−3.71 (m, 2 H), 3.44−3.55 (m, 2 H), 3.36 (m, 1 H), 2.20−2.28 (m, 3 H), 1.99−2.18 (m, 2 H), 1.37 (t, J = 6 Hz, 3 H), 1.29 (t, J = 6 Hz, 3 H), 0.98 (m, 3 H); ^{13}C NMR (150 MHz, DMSO-d_6) δ 171.7, 153.9, 153.8, 152.1, 144.7, 139.4, 137.5, 124.7, 109.2, 44.8, 44.2, 44.2, 40.5, 38.3, 27.4, 26.9, 15.5, 15.4, 10.5, 9.4; HRMS (EI) calcd for $C_{20}H_{29}N_8O$ $[M + H]^+$, 397.2464; found, 397.2464.

*1-((S)-3-(8-(1-Ethyl-5-methyl-1H-pyrazol-4-yl)-9-propyl-9H-purin-6-ylamino)pyrrolidin-1-yl)propan-1-one (**2d**).* A mixture of 4,6-dichloropyrimidin-5-amine (3.0 g, 18 mmol) and propan-1-amine (2.7 g, 46 mmol) in IPA (20 mL) and water (10 mL) was heated at 80 °C for 16 h. The reaction mixture was concentrated and purified by chromatography on silica gel (20:1 DCM/MeOH) to give 6-chloro-N4-propylpyrimidine-4,5-diamine (3.0 g, 88%) as a yellow solid. MS (EI) calcd for $C_7H_{12}ClN_4$ $[M + H]^+$, 187; found, 187. To a solution of 6-chloro-N4-propylpyrimidine-4,5-diamine (600 mg, 3.2 mmol) and 6-methylnicotinaldehyde (1.3 g, 9.6 mmol) in DMF (10 mL) was added $FeCl_3$·$6H_2O$ (216 mg, 0.8 mmol) slowly at RT. The resulting mixture was heated at 80 °C under air for 16 h. The reaction was quenched with water (10 mL) and extracted with DCM. The organic layer was washed with brine, dried (Na_2SO_4), filtered, and concentrated. The residue was purified by chromatography on silica gel (10:1 DCM/MeOH) to give 6-chloro-8-(1-ethyl-5-methyl-1*H*-pyrazol-4-yl)-9-propyl-9*H*-purine (500 mg, 50%) as a yellow solid. MS (EI) calcd for $C_{14}H_{18}N_6$ $[M + H]^+$, 305; found, 305.

6-Chloro-8-(1-ethyl-5-methyl-1*H*-pyrazol-4-yl)-9-propyl-9*H*-purine (200 mg, 0.65 mmol) and (*S*)-1-(3-aminopyrrolidin-1-yl)propan-1-one (370 mg, 2.62 mmol) were dissolved in a mixture of t-BuOH/DIPEA (1:1, 4 mL). The reaction mixture was heated to 80 °C for 36 h under an N_2 atmosphere. The reaction mixture was cooled to RT, and the solvent was removed under reduced pressure. The residue was purified by reverse-phase chromatography (gradient of MeCN/water with 10 mM NH_4HCO_3) to provide 1-((*S*)-3-(8-(1-ethyl-5-methyl-1*H*-pyrazol-4-yl)-9-propyl-9*H*-purin-6-ylamino)pyrrolidin-1-yl)propan-1-one (**2d**). ^{1}H NMR (400 MHz, DMSO-d_6) δ 8.25 (s, 1 H), 7.81−7.90 (m, 2 H), 4.70 (s, 1 H), 4.10−4.25 (m, 4 H), 3.30−3.85 (m, 4 H), 2.50(s, 3 H), 2.00−2.30 (m, 4 H), 1.15−1.25 (m, 2 H), 1.36 (t, J = 7.2 Hz, 3 H), 0.95 (t, J = 7.2 Hz, 3 H), 0.75 (t, J = 8.0 Hz, 3 H). HRMS (EI) calcd for $C_{21}H_{31}N_8O$ $[M + H]^+$, 411.2621; found, 411.2627.

*1-((S)-3-(9-(2,2-Difluoroethyl)-8-(1-ethyl-5-methyl-1H-pyrazol-4-yl)-9H-purin-6-ylamino)pyrrolidin-1-yl)propan-1-one (**2e**).* Prepared in a fashion similar to that used for the synthesis of **2d**. ^{1}H NMR (500 MHz, DMSO-d_6) δ 8.27 (s, 1 H), 7.98 (br, 1 H), 7.83 (s, 1 H), 6.39 (m, 1 H), 4.81 (m, 1 H), 4.64 (m, 2 H), 4.18 (q, J = 7.2 Hz, 2 H), 3.82 (m, 1 H), 3.61−3.73 (m, 1 H), 3.50 (m, 1 H), 3.37 (m, 1 H), 2.47 (m, 3 H), 2.24 (m, 2 H), 2.00−2.20 (m, 2 H), 1.36 (t, J = 7.2 Hz, 3 H), 0.98 (q, J = 7.5 Hz, 3 H); HRMS (EI) calcd for $C_{20}H_{27}F_2N_8O$ $[M + H]^+$, 433.2276; found, 433.2271.

*1-((S)-3-(8-(1-Ethyl-5-methyl-1H-pyrazol-4-yl)-9-(2,2,2-trifluoroethyl)-9H-purin-6-ylamino)pyrrolidin-1-yl)propan-1-one (**2f**).* A mixture of (*S*)-1-(3-(8-(1-ethyl-5-methyl-1*H*-pyrazol-4-yl)-9*H*-purin-6-ylamino)pyrrolidin-1-yl)propan-1-one (**2a**; 100 mg, 0.27 mmol) and K_2CO_3 (75 mg, 0.54 mmol) in DCM (5 mL) was cooled to 0 °C and then treated with 2,2,2-trifluoroethyl trifluoromethanesulfonate (74 mg, 0.32 mmol). The reaction mixture was stirred for 16 h at 25 °C under an N_2 atmosphere. The mixture was filtered and concentrated. The residue was purified by reverse-phase chromatography (gradient of MeCN/water with 0.05% TFA) to provide 1-((*S*)-3-(8-(1-ethyl-5-methyl-1*H*-pyrazol-4-yl)-9-(2,2,2-trifluoroethyl)-9*H*-purin-6-ylamino)pyrrolidin-1-yl)propan-1-one (**2f**, 12 mg; 9%) as a white solid. ^{1}H NMR (400 MHz, CD_3OD) δ 8.42 (s, 1 H), 7.91 (s, 1 H), 5.14 (s, 2 H), 4.31 (t, J = 7.2 Hz, 2 H), 3.89−4.02 (m, 1 H), 3.61−3.82 (m, 3 H), 2.53 (s, 3 H), 2.37−2.47 (m, 3 H), 2.15−2.27 (m, 2 H), 1.49 (q, J = 7.2 Hz, 3 H), 1.17 (q, J = 7.2 Hz, 3 H); HRMS (EI) calcd $C_{20}H_{25}F_3N_8O$ $[M + H]^+$, 451.2182; found, 451.2184.

*(S)-1-(3-((9-Cyclopropyl-8-(1-ethyl-5-methyl-1H-pyrazol-4-yl)-9H-purin-6-yl)amino)pyrrolidin-1-yl)propan-1-one (**2g**).* Prepared in a fashion similar to that used for the synthesis of **2d**. ^{1}H NMR (600 MHz, DMSO-d_6) δ 8.34 (s, 1 H), 8.05 (s, 1 H), 4.15 (q, J = 6 Hz, 2 H), 3.78 (m, 1 H), 3.67 (m, 1 H), 3.52−3.62 (m, 2 H), 3.47 (m, 2 H), 3.37 (m, 1 H), 2.56 (s, 3 H), 2.16−2.24 (m, 2 H), 2.09 (m, 1 H), 2.00 (m, 1 H), 1.33 (t, J = 6 Hz, 3 H), 1.11 (m, 2 H), 0.94 (m, 3 H), 0.88 (m, 2 H), HRMS (EI) calcd for $C_{21}H_{29}F_2N_8O$ $[M + H]^+$, 409.2464; found, 409.2471.

*1-((S)-3-(9-(Cyclopropylmethyl)-8-(1-ethyl-5-methyl-1H-pyrazol-4-yl)-9H-purin-6-ylamino)pyrrolidin-1-yl)propan-1-one (**2h**).* Prepared in a fashion similar to that used for the synthesis of **2d**. ^{1}H NMR (500 MHz, DMSO-d_6) δ 8.23 (s, 1 H), 7.75−7.99 (m, 2 H), 4.79 (s, 1 H), 4.18 (q, J = 7.2 Hz, 2 H), 4.03−4.15 (m, 2 H), 3.67 (m, 1 H), 3.41−3.60 (m, 2 H), 3.37 (m, 1 H), 2.49 (s, 3 H), 2.24 (m, 2 H), 1.94−2.19 (m, 2 H), 1.36 (t, J = 7.2 Hz, 3 H), 1.12 (m, 1 H), 0.99 (m, 3 H), 0.40 (m, 2 H), 0.28 (m, 2 H); HRMS (EI) calcd for $C_{22}H_{31}N_8O$ $[M + H]^+$, 423.2621; found, 423.2614.

*(S)-1-(3-(8-(1-Ethyl-2-methyl-1H-pyrrol-3-yl)-9-methyl-9H-purin-6-ylamino)pyrrolidin-1-yl)propan-1-one (**2i**).* A solution of 6-chloro-N4-methylpyrimidine-4,5-diamine (2.0 g, 13 mmol) and 1-ethyl-2-methyl-1*H*-pyrrole-3-carbaldehyde (1.7 g, 13 mmol) in DMF (15 mL) was treated with $FeCl_3$·$6H_2O$ (1.0 g, 3.8 mmol) at RT. The resulting mixture was heated at 90 °C for 16 h. The reaction was quenched with water and extracted with EtOAc. The organic layers were washed with brine, dried over Na_2SO_4, filtered, and concentrated. The residue was purified by column chromatography on silica gel (3:1 petroleum ether/EtOAc) to give 6-chloro-8-(1-ethyl-2-methyl-1*H*-pyrrol-3-yl)-9-methyl-9*H*-purine (1.4 g, 37%) as a yellow solid. MS (EI) calcd for $C_{13}H_{15}ClN_5$ $[M + H]^+$, 276; found, 276.

To a solution of 6-chloro-8-(1-ethyl-2-methyl-1*H*-pyrrol-3-yl)-9-methyl-9*H*-purine (50 mg, 0.18 mmol) in t-BuOH (5 mL) were added (*S*)-1-(3-aminopyrrolidin-1-yl)propan-1-one (51 mg, 0.36 mmol) and DIPEA (0.16 mL, 0.9 mmol) at RT. The reaction mixture was heated to 80 °C for 36 h under a N_2 atmosphere. The reaction mixture was concentrated, and the residue was purified by reverse-phase chromatography (gradient of MeCN/water with 10 mM NH_4CO_3) to provide **2i** (40 mg, 0.10 mmol, 59%) as a white solid. ^{1}H NMR (400 MHz, DMSO-d_6) δ 8.20 (s, 1 H), 7.65−7.75 (m, 1 H), 6.85−6.94 (m, 1 H), 6.43 (s, 1 H), 4.85 (br s, 1 H), 3.95 (q, J = 7.2 Hz, 2 H), 3.36−3.83 (m, 7 H), 2.40−2.50 (m, 3 H), 2.00−2.28

https://doi.org/10.1021/acs.jmedchem.1c00237
J. Med. Chem. 2021, 64, 5137−5156

(m, 4 H), 1.31 (t, J = 7.2 Hz, 3 H), 0.98 (q, J = 7.4 Hz, 3 H); HRMS (EI) calcd for $C_{20}H_{28}N_7O$ [M + H]$^+$, 382.2355; found, 382.2358.

*(S)-1-(3-((8-(2-(tert-Butyl)thiazol-5-yl)-9-methyl-9H-purin-6-yl)-amino)pyrrolidin-1-yl)propan-1-one (**2j**).* Prepared in a fashion similar to that used for the synthesis of **2b**. ^{1}H NMR (600 MHz, DMSO-d_6) δ 8.36 (br, 1 H), 8.31 (s, 1 H), 8.30 (s, 1 H), 4.60−4.74 (m, 1 H), 3.90 (s, 3 H), 3.75 (m, 1 H), 3.60−3.65 (m, 1 H), 3.43−3.49 (m, 2 H), 3.34 (m, 1 H), 2.17−2.24 (m, 2 H), 2.09 (m, 1 H), 1.40 (s, 9 H), 0.93 and 0.95 (2 t, J = 6 Hz, 3 H); HRMS (EI) calcd for $C_{20}H_{28}N_7OS$ [M + H]$^+$, 414.2079; found, 424.2079.

*9-Methyl-8-(2-methylpyrimidin-5-yl)-N-[(3S)-1-propanoylpyrrolidin-3-yl]-9H-purin-6-amine (**2k**).* Prepared in a fashion similar to that used for the synthesis of **2b**, in which intermediate **IX** was used as the chloropurine precursor. $[\alpha]_D$ = +42° (c 0.5, MeOH); ^{1}H NMR (600 MHz, DMSO-d_6) δ 9.19 (s, 2 H), 8.41−8.09 (m, 2 H), 4.77 (m, 1 H), 3.87 (s, 3 H), 3.79, 3.50 (m, 1 H), 3.73−3.62 (m, 1 H), 3.51 (m, 1 H), 3.36 (m, 1 H), 2.74 (s, 3 H), 2.24 (m, 2 H), 2.10 (m, 1 H), 2.05 (m, 1 H), 0.99 (m, 3 H); ^{13}C NMR (150 MHz, DMSO-d_6) δ 171.7, 168.4, 157.0 (2C), 154.4, 153.1, 151.4, 145.6, 122.1, 119.8, 50.8, 44.7, 44.1, 30.5, 27.4, 27.0, 26.2, 9.4; HRMS (EI) calcd for $C_{18}H_{23}N_8O$ [M + H]$^+$, 367.1995; found, 367.1999.

*(S)-1-(3-((9-Ethyl-8-(2-methylpyrimidin-5-yl)-9H-purin-6-yl)-amino)pyrrolidin-1-yl)propan-1-one (**2l**).* Prepared in a fashion similar to that used for the synthesis of **2b**, in which intermediate **X** was used as the chloropurine precursor. $[\alpha]_D$ = +28° (c 0.5, MeOH); ^{1}H NMR (600 MHz, DMSO-d_6) δ 9.08 (s, 2 H), 8.58 (s, 1 H), 8.35 (s, 1 H), 4.69 (m, 1 H), 4.28 (m, 2 H), 3.75 (m, 1 H), 3.59−3.66 (m, 1 H), 3.44−3.49 (m, 1 H), 3.32−3.37 (m, 1 H), 2.71 (s, 3 H), 2.16−2.23 (m, 2 H), 2.08 (m, 1 H), 2.01 (m, 1 H), 1.27 (t, J = 10 Hz, 3 H), 0.94 (m, 3 H); ^{13}C NMR (125 MHz, DMSO-d_6) δ 171.7, 168.6, 157.0 (2C), 154.2, 153.2, 150.8, 145.0, 124.7, 122.3, 51.2, 44.7, 44.1, 38.9, 27.4, 26.9, 26.2, 15.5, 9.4; HRMS (EI) calcd for $C_{19}H_{25}N_8O$ [M + H]$^+$, 381.2151; found, 381.2154.

*8-(2-Methylpyrimidin-5-yl)-N-[(3S)-1-propanoylpyrrolidin-3-yl]-9-propyl-9H-purin-6-amine (**2m**).* Prepared in a fashion similar to that used for the synthesis of **2l**. ^{1}H NMR (500 MHz, DMSO-d_6) δ 9.13 (s, 2 H), 8.16−8.39 (m, 2 H), 4.77 (m, 1 H), 4.26 (t, J = 7.3 Hz, 2 H), 3.62−3.85 (m, 1 H), 3.51 (m, 2 H), 3.35−3.41 (m, 1 H), 2.75 (s, 3 H), 2.24 (m, 2 H), 1.99−2.19 (m, 2 H), 1.69 (m, 2 H), 0.98 (t, J = 7.5 Hz, 3 H), 0.75 (t, J = 7.3 Hz, 3 H); HRMS (EI) calcd for $C_{20}H_{27}N_8O$ [M + H]$^+$, 395.2308; found, 395.2311.

*9-Methyl-8-(6-methylpyridin-3-yl)-N-[(3S)-1-propanoylpyrrolidin-3-yl]-9H-purin-6-amine (**2n**).* A solution of 6-chloro-N4-methylpyrimidine-4,5-diamine (150 mg, 0.95 mmol) and 6-methylnicotinaldehyde (126 mg, 1.0 mmol) in DMF (3 mL) was treated with $FeCl_3$·$6H_2O$ (64 mg, 0.24 mmol). The mixture was heated to 90 °C for 16 h. The reaction was quenched with water and extracted with DCM. The organic layer was washed with brine, dried (Na_2SO_4), filtered, and concentrated. The residue was purified by chromatography on SiO_2 (10:1 DCM/MeOH) to give 6-chloro-9-methyl-8-(6-methylpyridin-3-yl)-9H-purine (80 mg, 33%) as a yellow solid. MS (EI) calcd for $C_{12}H_{11}ClN_5$ [M + H]$^+$, 260; found, 260.

6-Chloro-9-methyl-8-(6-methylpyridin-3-yl)-9H-purine (80 mg, 0.31 mmol) and (*S*)-1-(3-aminopyrrolidin-1-yl)propan-1-one (48 mg, 0.34 mmol) were added to a mixture of t-BuOH/DIPEA (1:1, 3 mL). The reaction mixture was heated to 80 °C for 36 h. The reaction mixture was cooled to RT and concentrated. The residue was purified by reverse-phase chromatography (gradient of MeCN/water with 10 mM NH_4HCO_3) to provide 9-methyl-8-(6-methylpyridin-3-yl)-*N*-[(3*S*)-1-propanoylpyrrolidin-3-yl]-9H-purin-6-amine (20 mg, 18%) as a yellow solid. ^{1}H NMR (400 MHz, CD_3OD) δ 9.2 (s, 1 H), 8.74 (d, J = 8.0 Hz, 1 H), 8.46 (d, J = 4.0 Hz, 1 H), 7.94 (d, J = 8.0 Hz, 1 H), 5.50−5.60 and 4.70−4.80 (m, 1 H), 4.05 (s, 3 H), 3.69−3.74 (m, 4 H), 2.85 (s, 3 H), 2.38−2.45 (m, 4 H), 1.50 (t, J = 8.0 Hz, 3 H). HRMS (EI) calcd for $C_{19}H_{24}N_7O$ [M + H]$^+$, 366.2042; found, 366.2044.

*(S)-1-(3-((9-Methyl-8-(6-(trifluoromethyl)pyridin-3-yl)-9H-purin-6-yl)amino)pyrrolidin-1-yl)propan-1-one (**2o**).* A solution of propionyl chloride (2.19 g, 23.6 mmol) in dry DCM (3 mL) was treated with a solution of (*S*)-*tert*-butyl-pyrrolidin-3-ylcarbamate (4.00 g, 21.5 mmol) and triethylamine (4.34 g, 43.0 mmol) in dry DCM (17 mL) portionwise at 0 °C. The reaction mixture was allowed to warm to RT and stirred for 3 h. Then, water (30 mL) was added, the mixture was extracted with DCM, and the organic layer was dried (Na_2SO_4), filtered, and concentrated to obtain (*S*)-*tert*-butyl-(1-propionylpyrrolidin-3-yl)carbamate, which was used in the next step without further purification. A solution of (*S*)-*tert*-butyl-(1-propionylpyrrolidin-3-yl)carbamate (4.5 g, 18 mmol) in dioxane (5 mL) was treated with 1 N HCl in dioxane (10 mL), and the mixture was stirred for 2 h at RT. The pH of the mixture was adjusted to 9−10 with saturated aqueous Na_2CO_3. The aqueous layer was dried in vacuo and the residue was extracted with MeOH and concentrated to obtain (*S*)-1-(3-aminopyrrolidin-1-yl)propan-1-one, which was used in the next step without further purification.

6-Chloro-9-methyl-8-(6-(trifluoromethyl)pyridin-3-yl)-9H-purine (**XI**, 50 mg, 0.16 mmol) and (S)-1-(3-aminopyrrolidin-1-yl)propan-1-one (28 mg, 0.19 mmol) were added to a mixture of 1:1 t-BuOH/DIEA (2 mL). The reaction mixture was heated at 75 °C for 3 days. The resulting mixture was cooled to RT, and the solvent evaporated to afford the crude residue which was purified by chromatography on SiO_2 (MeOH/DCM = 1/20) to give **2o** as a white solid. ^{1}H NMR (400 MHz, $CDCl_3$) δ 9.19 (s, 1 H), 8.49 (m, 1 H), 8.35 (m, 1 H), 7.91 (m, 1 H), 5.99 (m, 1 H), 4.99 (s, 1 H), 3.97−4.00 (m, 3 H), 3.76−3.95 (m, 1 H), 3.63−3.70 (m, 2 H), 3.48−3.51 (m, 1 H), 2.28−2.48 (m, 3 H), 2.16−2.20 (m, 1 H), 1.16−1.21 (m, 3 H); HRMS (EI) calcd for $C_{19}H_{21}F_3N_7O$ [M + H]$^+$, 420.1759; found, 420.1764.

*8-(6-Methoxypyridin-3-yl)-9-methyl-N-[(3S)-1-propanoylpyrrolidin-3-yl]-9H-purin-6-amine (**2p**).* Prepared in a fashion similar to that used for the synthesis of **2k**. ^{1}H NMR (500 MHz, DMSO-d_6) δ 8.68 (s, 1 H), 8.30 (s, 1 H), 8.17−8.22 (m, 1 H), 8.10 (br d, 1 H), 7.03 (d, J = 8.6 Hz, 1 H), 4.80 (br, 1 H), 3.95 (s, 3 H), 3.86 (s, 3 H), 3.61−3.73 (m, 1 H), 3.43−3.56 (m, 2 H), 3.35−3.40 (m, 1 H), 2.24 (m, 2 H), 1.96−2.19 (m, 2 H), 0.98 (q, J = 7.5 Hz, 3 H); HRMS (EI) calcd for $C_{19}H_{24}N_7O_2$ [M + H]$^+$, 382.1991; found, 382.2003.

*8-(5-Fluoro-6-methoxypyridin-3-yl)-9-methyl-N-[(3S)-1-propanoylpyrrolidin-3-yl]-9H-purin-6-amine (**2q**).* Prepared in a fashion similar to that used for the synthesis of **2k**. ^{1}H NMR (500 MHz, DMSO-d_6) δ 8.50 (s, 1 H), 8.31 (s, 1 H), 8.18 (m, 2 H), 4.79 (s, 1 H), 4.05 (s, 3 H), 3.83 (s, 3 H), 3.62−3.73 (m, 1 H), 3.50 (m, 2 H), 3.35 (m, 1 H), 2.24 (m, 2 H), 2.08 (m, 2 H), 0.98 (t, J = 7.6 Hz, 3 H); HRMS (EI) calcd for $C_{19}H_{23}FN_7O_2$ [M + H]$^+$, 400.1897; found, 400.1906.

*(S)-1-(3-((8-(6-Methoxy-5-methylpyridin-3-yl)-9-methyl-9H-purin-6-yl)amino)pyrrolidin-1-yl)propan-1-one (**2r**).* Prepared in a fashion similar to that used for the synthesis of **2b**. ^{1}H NMR (600 MHz, DMSO-d_6) δ 8.63 (br, 1 H), 8.48 (s, 1 H), 8.34 (s, 1 H), 8.01 (s, 1 H), 4.61−4.71 (br m, 1 H), 3.93 (s, 3 H), 3.81 (s, 3 H), 3.60−3.75 (m, 1 H), 3.44−3.50 (m, 2 H), 3.35 (m, 1 H), 2.19 (s, 3 H), 2.16−2.25 (m, 2 H), 2.00−2.20 (m, 2 H), 0.95, 0.93 (2 t, J = 6 Hz, 3 H); HRMS (EI) calcd for $C_{20}H_{26}N_7O_2$ [M + H]$^+$, 396.2148; found, 396.2148.

*(S)-1-(3-((9-Ethyl-8-(2-methylpyrimidin-5-yl)-9H-purin-6-yl)oxy)-pyrrolidin-1-yl)propan-1-one (**3b**).* To a solution of (*S*)-*tert*-butyl-3-hydroxypyrrolidine-1-carboxylate (4.0 g, 21 mmol) in THF (80 mL), 60% NaH in mineral oil (1.5 g, 38 mmol) was added. The mixture was stirred at 0 °C for 30 min, and then intermediate **X** (5.0 g, 18 mmol) was added. The solution was stirred at RT for 15 h, then cooled, diluted with water, and extracted with EtOAc. The combined organic layers were concentrated under reduced pressure to give (*S*)-*tert*-butyl-3-(9-ethyl-8-(2-methylpyrimidin-5-yl)-9H-purin-6-yloxy)-pyrrolidine-1-carboxylate (7.0 g, 90%). MS (EI) calcd for $C_{21}H_{28}N_7O_3$ [M + H]$^+$, 426; found 426.

To a solution of (*S*)-*tert*-butyl-3-(9-ethyl-8-(2-methylpyrimidin-5-yl)-9H-purin-6-yloxy)pyrrolidine-1-carboxylate (7.0 g, 16 mmol) in DCM (80 mL) was added TFA (20 mL), and the reaction stirred at RT for 2 h. The mixture was cooled, saturated aqueous $NaHCO_3$ was added, and the mixture was extracted with DCM. The combined organic extracts were concentrated under reduced pressure to give (*S*)-9-ethyl-8-(2-methylpyrimidin-5-yl)-6-(pyrrolidin-3-yloxy)-9H-pu-

https://doi.org/10.1021/acs.jmedchem.1c00237
J. Med. Chem. 2021, 64, 5137−5156

rine (5 g, 93%). MS (EI) calcd for $C_{16}H_{20}N_7O$ $[M + H]^+$, 326; found, 326.

A solution of (*S*)-9-ethyl-8-(2-methylpyrimidin-5-yl)-6-(pyrrolidin-3-yloxy)-9*H*-purine (35 mg, 0.088 mmol) in DMF (1 mL) was treated with Hunig's base (0.10 mL, 0.57 mmol) followed by propionyl chloride (15 mg, 0.16 mmol), stirred for 1 h, filtered, and purified by reverse-phase chromatography (gradient of MeCN/water with 0.1% TFA) to provide **3b** (19 mg, 44%). ^{1}H NMR (600 MHz, CD_3OD) δ 9.10 (s, 2 H), 8.55 (s, 1 H), 6.00 (m, 1 H), 4.42 (m, 2 H), 3.70−3.90 (m, 4 H), 2.80 (s, 3 H), 2.30−2.45 (m, 4 H), 1.43 (t, J = 9 Hz, 3 H), 1.12 (m, 3 H); MS (EI) calcd for $C_{19}H_{25}N_7O_2$ $[M + H]^+$, 383; found, 383.

*(S)-Cyclopropyl(3-((9-ethyl-8-(2-methylpyrimidin-5-yl)-9H-purin-6-yl)amino)pyrrolidin-1-yl)methanone (**3c**).* A solution of (*S*)-*tert*-butyl-pyrrolidin-3-ylcarbamate (100 g, 537 mmol) in EtOAc (1 L) was treated dropwise at 0 °C over a 1 h period with NEt_3 (79 mL, 569 mmol) followed by cyclopropanecarbonyl chloride (50 mL, 548 mmol) while maintaining an internal temperature of less than 10 °C. The mixture was stirred for another 15 min and then washed with water. The aqueous layer was extracted with EtOAc, and the combined organic layers dried (Na_2SO_4) and filtered. The organic layer was then treated with $TsOH·H_2O$ (112 g, 591 mmol), and the mixture was stirred at 47 °C for 15 h. The precipitate that then formed was filtered, collected, and dried with a flow of nitrogen giving 153 g (87%) of (*S*)-(3-aminopyrrolidin-1-yl)(cyclopropyl)methanone 4-methylbenzenesulfonate salt. ^{1}H NMR (600 MHz, CD_3OD) δ 7.68 (d, J = 10 Hz, 2 H), 7.21 (d, J = 10 Hz, 2 H), 4.02 (m, 1 H), 3.81−3.91 (m, 2 H), 3.72 (m, 1 H), 3.52 (m, 1 H), 2.43 (m, 1 H), 2.35 (s, 3 H), 2.14 (m, 1 H), 1.78 (m, 1 H), 0.81−0.91 (m, 4 H).

A mixture containing 6-chloro-9-ethyl-8-(2-methylpyrimidin-5-yl)-9*H*-purine (**X**, 120 g, 437 mmol), (*S*)-(3-aminopyrrolidin-1-yl)-(cyclopropyl)methanone-4-methylbenzenesulfonate salt (157 g, 481 mmol), and Na_2CO_3 (162 g, 1530 mmol) in *tert*-amyl-OH (1 L) was stirred at 90 °C for 42 h. The mixture was poured into 1.6 L of water and extracted with DCM (3 × 450 mL). The organic layer was dried (Na_2SO_4) and concentrated. The residue was then taken-up in 1.6 L of hexane, stirred overnight, and filtered. The solid was dried overnight with a flow of nitrogen, giving 150 g (88%) of (*S*)-cyclopropyl(3-((9-ethyl-8-(2-methylpyrimidin-5-yl)-9*H*-purin-6-yl)-amino)pyrrolidin-1-yl)methanone (**3c**). $[\alpha]_D$ = +42° (c 2.0, MeOH); ^{1}H NMR (600 MHz, CD_3OD) δ 9.08 (s, 2 H), 8.31 (m, 1 H), 4.80−4.95 (m, 1 H), 4.37 (m, 2 H), 3.90−4.15 (m, 1 H), 3.79−3.87 (m, 1 H), 3.64−3.74 (m, 1 H), 3.52−3.59 (m, 1 H), 2.78 (s, 3 H), 2.30−2.40 (m, 1 H), 2.07−2.24 (m, 1 H), 1.73−1.84 (m, 1 H), 1.40 (t, J = 6 Hz, 3 H), 0.78−0.88 (m, 4 H); ^{13}C NMR (125 MHz, DMSO-d_6) δ 171.4, 168.6, 157.0, 154.4, 153.2, 150.9, 145.0, 144.9, 122.3, 120.0, 51.4, 50.1, 44.8, 38.9, 30.5, 26.2, 15.5, 12.3, 7.5, 7.4; HRMS (EI) calcd for $C_{20}H_{25}N_8O$ $[M + H]^+$, 393.2151; found, 393.2153.

*(S)-Cyclopropyl(3-((9-ethyl-8-(2-methylpyrimidin-5-yl)-9H-purin-6-yl)oxy)pyrrolidin-1-yl)methanone (**3d**).* To a solution of (*S*)-*tert*-butyl-3-hydroxypyrrolidine-1-carboxylate (4.0 g, 21 mmol) in THF (80 mL), 60% NaH in mineral oil (1.5 g, 38 mmol) was added. The mixture was stirred at 0 °C for 30 min, and then intermediate **X** (5.0 g, 18 mmol) was added. The solution was stirred at RT for 15 h, then cooled, diluted with water, and extracted with EtOAc. The combined organic layers were concentrated under reduced pressure to give (*S*)-*tert*-butyl-3-(9-ethyl-8-(2-methylpyrimidin-5-yl)-9*H*-purin-6-yloxy)-pyrrolidine-1-carboxylate (7.0 g, 90%). MS (EI) calcd for $C_{21}H_{28}N_7O_3$ $[M + H]^+$, 426; found 426.

To a solution of (*S*)-*tert*-butyl-3-(9-ethyl-8-(2-methylpyrimidin-5-yl)-9*H*-purin-6-yloxy)pyrrolidine-1-carboxylate (7.0 g, 16 mmol) in DCM (80 mL) was added TFA (20 mL), and the reaction was stirred at RT for 2 h. The mixture was cooled, saturated aqueous $NaHCO_3$ was added, and the mixture was extracted with DCM. The combined organic extracts were concentrated under reduced pressure to give (*S*)-9-ethyl-8-(2-methylpyrimidin-5-yl)-6-(pyrrolidin-3-yloxy)-9*H*-purine (5 g, 93%). MS (EI) calcd for $C_{16}H_{20}N_7O$ $[M + H]^+$, 326; found, 326.

To a solution of cyclopropanecarboxylic acid (27 mg, 0.31 mmol) in DMF (2 mL) was added HATU (88 mg, 0.23 mmol) and 4-methylmorpholine (0.034 mL, 0.31 mmol). The mixed solution was stirred at RT for 15 min, then (*S*)-9-ethyl-8-(2-methylpyrimidin-5-yl)-6-(pyrrolidin-3-yloxy)-9*H*-purine (50 mg, 0.15 mmol) was added, and the solution was stirred at RT for 15 h. The mixture was cooled, water was added, and the mixture was extracted with EtOAc. The combined organic extracts were concentrated under reduced pressure. The residue was purified by preparative reverse-phase HPLC, eluting with MeCN/water with 0.05% TFA, to give **3d** (49 mg, 81%). $[\alpha]_D$ = +34° (c 0.5, MeOH); ^{1}H NMR (400 MHz, DMSO-d_6) δ 9.23 (s, 2 H), 8.56 (s, 1 H), 5.87−5.98 (m, 1 H), 4.37 (m, 2 H), 3.70−4.08 (m, 2 H), 3.39−3.67 (m, 2 H), 2.76 (s, 3 H), 2.24−2.51 (m, 2 H), 1.75−1.85 (m, 1 H), 1.35 (m, 3 H), 0.57−0.67 (m, 4 H); ^{13}C NMR (150 MHz, DMSO-d_6) δ 171.6, 169.0, 159.6, 157.2, 154.1, 152.1, 148.2, 146.5, 124.8, 121.8, 76.3, 54.6, 44.7, 33.7, 30.8, 26.2, 15.5, 12.4, 7.6, 7.3; HRMS (EI) calcd for $C_{20}H_{24}N_7O_2$ $[M + H]^+$, 394.1991; found, 394.1993.

*(S)-Cyclobutyl(3-((9-ethyl-8-(2-methylpyrimidin-5-yl)-9H-purin-6-yl)amino)pyrrolidin-1-yl)methanone (**3e**).* A 250 mL flask containing 6-chloro-9-ethyl-8-(2-methylpyrimidin-5-yl)-9*H*-purine (5.0 g, 18 mmol) and *tert*-butyl-(*S*)-3-aminopyrrolidine-1-carboxylate (4.8 g, 22 mmol) in DMF (100 mL) was treated with Hunig's base (20 mL, 120 mmol). The mixture was stirred at 65 °C for 48 h. The solvent was evaporated, and the residue was purified by chromatography on SiO_2 (gradient of 0−10% MeOH/DCM) to afford (*S*)-*tert*-butyl-3-((9-ethyl-8-(2-methylpyrimidin-5-yl)-9*H*-purin-6-yl)amino)-pyrrolidine-1-carboxylate (6.7 g, 87% yield). ^{1}H NMR (600 MHz, DMSO-d_6) δ 9.08 (s, 2 H), 8.28 (s, 1 H), 8.18 (s, 1 H), 4.67 (m, 1 H), 4.26 (m, 2 H), 3.56 (m, 1 H), 3.42 (m, 1 H), 3.25 (m, 2 H), 2.70 (s, 3 H), 2.11 (m, 1 H), 1.99 (m, 1 H), 1.34 and 1.36 (2s, 9 H), 1.26 (m, 3 H); MS (EI) calcd for $C_{21}H_{29}N_8O_2$ $[M + H]^+$, 425; found, 425.

A mixture of (*S*)-*tert*-butyl-3-((9-ethyl-8-(2-methylpyrimidin-5-yl)-9*H*-purin-6-yl)amino)pyrrolidine-1-carboxylate (6.7 g, 16 mmol) in dioxane (80 mL) was treated with a 4 M solution of HCl in dioxane (14 mL, 56 mmol). The resulting slurry was stirred overnight and concentrated to dryness to provide (*S*)-9-ethyl-8-(2-methylpyrimidin-5-yl)-*N*-(pyrrolidin-3-yl)-9*H*-purin-6-amine, 2HCl (6.4 g, 16 mmol, 100% yield). MS (EI) calcd for $C_{16}H_{21}N_8$ $[M + H]^+$, 325; found, 325.

A mixture of (*S*)-9-ethyl-8-(2-methylpyrimidin-5-yl)-*N*-(pyrrolidin-3-yl)-9*H*-purin-6-amine, 2 HCl (120 mg, 0.30 mmol), cyclobutanecarboxylic acid (64 mg, 0.63 mmol), HATU (140 mg, 0.36 mmol), DMF (2.5 mL), and Hunig's base (0.40 mL, 2.3 mmol) was stirred at RT for 18 h. The mixture was filtered and purified by reverse-phase chromatography (gradient of MeCN/water with 0.1% TFA) to afford (*S*)-cyclobutyl(3-((9-ethyl-8-(2-methylpyrimidin-5-yl)-9*H*-purin-6-yl)amino)pyrrolidin-1-yl)methanone (**3e**, 73 mg, 46% yield). ^{1}H NMR (600 MHz, DMSO-d_6) δ 9.08 (s, 2 H), 8.51 (br, 1 H), 8.33 (s, 1 H), 4.67 (m, 1 H), 4.27 (q, J = 6 Hz, 2 H), 3.64 (m, 1 H), 3.45−3.55 (m, 1 H), 3.38 (m, 1 H), 3.33 (m, 1 H), 3.15−3.25 (m, 1 H), 2.70 (s, 3 H), 1.90−2.15 (m, 6 H), 1.85 (m, 1 H), 1.69 (m, 1 H), 1.27 (t, J = 7 Hz, 3 H); HRMS (EI) calcd for $C_{21}H_{27}N_8O$ $[M + H]^+$, 407.2308; found, 407.2309.

*(S)-Cyclobutyl(3-((9-ethyl-8-(2-methylpyrimidin-5-yl)-9H-purin-6-yl)oxy)pyrrolidin-1-yl)methanone (**3f**).* Compound **3f** was prepared via a sequence analogous to the route used for the preparation of **3d**, replacing cyclopropyl carboxylic acid with cyclobutyl carboxylic acid. ^{1}H NMR (400 MHz, DMSO-d_6) δ 9.14 (s, 2 H), 8.62 (s, 1 H), 5.87 (m, 1 H), 4.39 (m, 2 H), 3.22−3.80 (m, 5 H), 2.76 (s, 3 H), 1.85−2.20 (m, 8 H), 1.33 (t, J = 7.2 Hz, 3 H); HRMS (EI) calcd for $C_{21}H_{26}N_7O_2$ $[M + H]^+$, 408.2148; found, 408.2144.

*cis-((S)-3-((9-Ethyl-8-(2-methylpyrimidin-5-yl)-9H-purin-6-yl)-amino)pyrrolidin-1-yl)((1S,3R)-3-methoxycyclobutyl)-methanone (**3g**).* A mixture of (*S*)-9-ethyl-8-(2-methylpyrimidin-5-yl)-*N*-(pyrrolidin-3-yl)-9*H*-purin-6-amine, 2HCl (79 mg, 0.20 mmol), 3-methoxycyclobutanecarboxylic acid (26 mg, 0.20 mmol), HATU (84 mg, 0.22 mmol), DMF (1 mL), and Hunig's base (0.24 mL, 1.4 mmol) was stirred at RT for 16 h. The mixture was filtered and purified by SFC (ES Industries Pyridyl Amide column, 21 × 250 mm; 70 mL/min; 10% MeOH in CO_2 with 0.25% Me_2NEt) to afford the *cis*- and *trans*-methoxycyclobutane products (22 and 24 mg, respectively). Data for the *cis* isomer **3g**, the second isomer eluted

https://doi.org/10.1021/acs.jmedchem.1c00237
J. Med. Chem. 2021, 64, 5137−5156

on the abovementioned column: $[\alpha]_D$ = +32° (c 0.5, MeOH); ^{1}H NMR (600 MHz, DMSO-d_6) δ 9.10 (s, 2 H), 8.30 (m, 1 H), 8.24 (m, 1 H), 4.71 (m, 1 H), 4.28 (m, 2 H), 3.40−3.75 (m, 4 H), 3.34 (m, 1 H), 3.07 and 3.09 (2 s, 3 H), 2.72 (s, 3 H), 2.73 (m, 1 H), 2.35 (m, 2 H), 2.15−2.30 (m, 1 H), 2.07 (m, 1 H), 1.85−2.00 (m, 2 H), 1.28 (m, 3 H); ^{13}C NMR (150 MHz, DMSO-d_6) δ 171.8, 168.6, 157.0 (2C), 154.5, 154.3, 153.2, 150.9, 122.3, 120.0, 70.1, 54.7, 51.0, 50.9, 44.4, 38.9, 32.9, 32.8, 28.7, 28.4, 26.2, 15.5; HRMS (EI) calcd for $C_{22}H_{29}N_8O_2$ $[M + H]^+$, 437.2413; found, 437.2419.

*((S)-3-((9-Ethyl-8-(2-methylpyrimidin-5-yl)-9H-purin-6-yl)oxy)-pyrrolidin-1-yl)((1S,3R)-3-methoxycyclobutyl)-methanone (**3h**).* A mixture containing *cis*-3-methoxycyclo-butanecarboxylic acid (22 mg, 0.17 mmol), Hunig's base (0.029 mL, 0.17 mmol), HATU (76 mg, 0.20 mmol), and (*S*)-9-ethyl-8-(2-methylpyrimidin-5-yl)-6-(pyrrolidin-3-yloxy)-9*H*-purine (60 mg, 0.17 mmol) in 2 mL of DMF was stirred for 4 h at RT and purified by reverse-phase chromatography (gradient of MeCN/water with 0.1% TFA) to provide the desired product, **3h** (37 mg, 48%). $[\alpha]_D$ = +36° (c 0.5, MeOH); ^{1}H NMR (600 MHz, DMSO-d_6) δ 9.10 (s, 2 H), 8.58 (s, 1 H), 5.85 (m, 1 H), 4.33 (m, 2 H), 3.81 (m, 1 H), 3.37 (m, 1 H), 3.51−3.74 (m, 3 H), 3.05 and 3.07 (2 s, 3 H), 2.78 (m, 1 H), 2.71 (s, 3 H), 2.13−2.39 (m, 4 H), 1.84−1.94 (m, 2 H), 1.29 (m, 3 H); ^{13}C NMR (125 MHz, DMSO-d_6) δ 172.0, 169.1, 159.5, 157.2, 154.1, 152.1, 148.1, 121.9, 121.4, 77.0, 75.5, 70.1, 54.7, 51.9, 44.2, 33.1, 32.7, 30.1, 28.6, 28.5, 26.2, 15.3; HRMS (EI) calcd for $C_{22}H_{28}N_7O_3$ $[M + H]^+$, 438.2253; found, 438.2256.

*(S)-(3,3-Difluorocyclobutyl)(3-((9-ethyl-8-(2-methylpyrimidin-5-yl)-9H-purin-6-yl)amino)pyrrolidin-1-yl)methanone (**3i**).* Prepared analogously to compound **3e**. Analytical data for **3i**: ^{1}H NMR (600 MHz, DMSO-d_6) δ 9.08 (s, 2 H), 8.51 (s, 1 H), 8.32 (s, 1 H), 4.73 (m, 1 H), 4.26 (m, 2 H), 3.72 (m, 1 H), 3.67 (m, 1 H), 3.57 (m, 1 H), 3.46 (m, 2 H), 3.38 (m, 1 H), 3.09 (m, 1 H), 2.74 (m, 2 H), 2.70 (s, 3 H), 1.97−2.22 (m, 3 H), 1.27 (m, 3 H); HRMS (EI) calcd for $C_{21}H_{25}F_2N_8O$ $[M + H]^+$, 443.2119; found, 443.2132.

*(S)-(3,3-Difluorocyclobutyl)(3-((9-ethyl-8-(2-methylpyrimidin-5-yl)-9H-purin-6-yl)oxy)pyrrolidin-1-yl)methanone (**3j**).* Prepared analogously to compound **3h**. Analytical data for **3j**: ^{1}H NMR (600 MHz, DMSO-d_6) δ 9.10 (s, 2 H), 8.57 (s, 1 H), 5.87 (m, 1 H), 4.33 (m, 2 H), 3.38−3.86 (m, 5 H), 3.09−3.19 (m, 2 H), 2.64−2.79 (m, 2 H), 2.72 (s, 3 H), 2.15−2.35 (m, 2 H), 1.29 (m, 3 H); HRMS (EI) calcd for $C_{21}H_{24}F_2N_7O_2$ $[M + H]^+$, 444.1959; found, 444.1959.

*(S)-(3-((9-Ethyl-8-(2-methylpyrimidin-5-yl)-9H-purin-6-yl)-amino)pyrrolidin-1-yl)(3-methoxyazetidin-1-yl)methanone (**3k**).* A mixture of (*S*)-9-ethyl-8-(2-methylpyrimidin-5-yl)-*N*-(pyrrolidin-3-yl)-9*H*-purin-6-amine, 2HCl (200 mg, 0.503 mmol) and CDI (163 mg, 1.01 mmol) was taken-up in THF (2.5 mL), and Hunig's base (0.26 mL, 1.5 mmol) was added. The reaction was stirred at 75 °C for 2 h. Next, 3:1 chloroform/IPA and sat'd NH_4Cl were added. The combined organics were washed with brine, dried ($MgSO_4$), and concentrated. Purification by chromatography on SiO_2 (50−100% 3:1 EtOAc:EtOH with 1% NH_4 in hexanes gave (*S*)-(3-((9-ethyl-8-(2-methylpyrimidin-5-yl)-9*H*-purin-6-yl)amino)pyrrolidin-1-yl)(1*H*-imidazol-1-yl)methanone (132 mg, 0.315 mmol, 63% yield). MS (EI) calcd for $C_{20}H_{23}N_{10}O$ $[M + H]^+$, 419; found, 419.

A vial was charged with (*S*)-(3-((9-ethyl-8-(2-methylpyrimidin-5-yl)-9*H*-purin-6-yl)amino)pyrrolidin-1-yl)(1*H*-imidazol-1-yl)-methanone (132 mg, 0.315 mmol), MeCN (4 mL) followed by iodomethane (0.079 mL, 1.3 mmol). The reaction mixture was stirred for 1 h at RT. The solvent was removed in vacuo, and the solid was triturated in ether and filtered to give an orange solid (*S*)-1-(3-((9-ethyl-8-(2-methylpyrimidin-5-yl)-9*H*-purin-6-yl)amino)pyrrolidine-1-carbonyl)-3-methyl-1*H*-imidazol-3-ium, HCl (142 mg, 0.302 mmol, 96% yield). MS (EI) calcd for $C_{21}H_{25}N_{10}O$ $[M + H]^+$, 433; found, 433.

(*S*)-1-(3-((9-Ethyl-8-(2-methylpyrimidin-5-yl)-9*H*-purin-6-yl)-amino)pyrrolidine-1-carbonyl)-3-methyl-1*H*-imidazol-3-ium (142 mg, 0.328 mmol) and 3-methoxyazetidine-HCl (34 mg, 0.39 mmol) in DMA (3 mL) were treated with Hunig's base (0.11 mL, 0.66 mmol) and stirred at 55 °C overnight. The mixture was taken-up in 3:1 chloroform/IPA and washed with sat'd $NaHCO_3$. The organic layer was dried ($MgSO_4$) and concentrated. The residue was dissolved in DMSO and purified by reverse-phase chromatography (gradient of MeCN/water with 0.1% TFA) to provide the desired product **3k** (38 mg, 26%). $[\alpha]_D$ = +38° (c 0.5, MeOH); ^{1}H NMR (600 MHz, DMSO-d_6) δ 9.11 (s, 2 H), 8.32 (m, 1 H), 8.23 (m, 1 H), 4.69 (m, 1 H), 4.29 (m, 2 H), 4.10 (m, 1 H), 4.02 (m, 2 H), 3.67 (m, 2 H), 3.59 (m, 1 H), 3.47 (m, 1 H), 3.31 (m, 2 H), 3.17 (s, 3 H), 2.74 (s, 3 H), 1.98−2.15 (m, 2 H), 1.30 (m, 3 H); ^{13}C NMR (150 MHz, DMSO-d_6) δ 168.6, 160.8, 157.0 (2C), 154.4, 153.2, 150.9, 144.9, 122.3, 120.0, 69.2, 57.4, 55.7, 51.8, 50.1, 45.2, 38.9, 30.7, 26.2, 26.0, 15.5; HRMS (EI) calcd for $C_{21}H_{28}N_8O_2$ $[M + H]^+$, 438.2366; found, 438.2372.

*(S)-(3-((9-Ethyl-8-(2-methylpyrimidin-5-yl)-9H-purin-6-yl)oxy)-pyrrolidin-1-yl)(3-methoxyazetidin-1-yl)methanone (**3l**).* To a solution of 3-methoxyazetidine, HCl (0.020 g, 0.17 mmol) in DCM (3.3 mL) and TEA (0.092 mL, 0.66 mmol) was added triphosgene (0.030 g, 0.10 mmol). The solution was stirred at RT for 1 h. In a separate reaction vessel, (*S*)-9-ethyl-8-(2-methylpyrimidin-5-yl)-6-(pyrrolidin-3-yloxy)-9*H*-purine (intermediate prepared for the synthesis of **3d**; 0.060 g, 0.17 mmol) was suspended in DCM (0.50 mL) along with TEA (0.050 mL, 0.36 mmol). The solution was stirred at RT for 1 h. This suspension was then added via a syringe to the first vessel, and the reaction was stirred at RT for 16 h. The solvent was then evaporated, and the crude reaction mixture was then resuspended in DMF (1.0 mL). An additional portion of TEA (0.10 mL) was added, and the reaction was heated to 50 °C for 72 h. The reaction vial was then cooled, diluted with DMSO (0.90 mL), and purified by reverse-phase preparative HPLC to afford the TFA salt of **3l**. The TFA salt was then dissolved in methanol and eluted through a 1g SiliPrepTM silicon-carbonate cartridge to afford neutral **3l** (9.9 mg, 14%). ^{1}H NMR (600 MHz, DMSO-d_6) δ 9.13 (s, 2 H), 8.59 (s, 1 H), 5.82 (s, 1 H), 4.35 (q, J = 7.2 Hz, 2 H), 4.04−4.17 (m, 2 H), 3.92−4.04 (m, 1 H), 3.61−3.78 (m, 3 H), 3.53 (d, J = 12.0 Hz, 1 H), 3.37−3.49 (m, 2 H), 3.16 (s, 3 H), 2.74 (s, 3 H), 2.11−2.31 (m, 2 H), 1.32 (t, J = 7.2 Hz, 3 H). MS (EI) calcd for $C_{21}H_{27}N_8O_3$ $[M + H]^+$ 439; found 439.

*(3(S)-((9-Ethyl-8-(2-methylpyrimidin-5-yl)-9H-purin-6-yl)amino)-pyrrolidin-1-yl)(tetrahydrofuran-3(R or S)-yl) methanone (**3m**).* A solution of (*S*)-9-ethyl-8-(2-methylpyrimidin-5-yl)-*N*-(pyrrolidin-3-yl)-9*H*-purin-6-amine (50 mg, 0.15 mmol) in DMF (2 mL) was treated with tetrahydrofuran-3-carboxylic acid (18 mg, 0.15 mmol), HATU (59 mg, 0.15 mmol), and Hunig's base (20 mg, 0.15 mmol). The mixture was stirred for 10 h and then purified by reverse-phase chromatography (gradient of MeCN/water with 0.05% NH_4OH to provide a diastereomeric mixture, which was then resolved using chiral column chromatography (Chiralpak IA column, eluting with MeOH/CO_2) to provide diastereomer 1 (15 mg, 46%) and diastereomer 2 (17 mg, 52%)). Analytical data for the first, more potent diastereomer **3m**: ^{1}H NMR (400 MHz, CD_3OD) δ 9.13 (s, 2 H), 8.36 (s, 1 H), 4.40 (m, 2 H), 4.02 (m, 1 H), 3.50−3.90 (m, 7 H), 3.10 (m, 1 H), 2.82 (s, 4 H), 2.10−2.22 (m, 4 H), 1.44 (m, 3 H); HRMS (EI) calcd for $C_{21}H_{27}N_8O_2$ $[M + H]^+$, 423.2257; found, 423.2263.

*((S)-3-((9-Ethyl-8-(2-methylpyrimidin-5-yl)-9H-purin-6-yl)oxy)-pyrrolidin-1-yl)(tetrahydrofuran-3(R or S)-yl)methanone (**3n**).* A solution of tetrahydrofuran-3-carboxylic acid (39 mg, 0.33 mmol) in DMF (2 mL) was treated with HATU (150 mg, 0.40 mmol), (*S*)-9-ethyl-8-(2-methylpyrimidin-5-yl)-6-(pyrrolidin-3-yloxy)-9*H*-purine, HCl (120 mg, 0.332 mmol), and Hunig's base (0.058 mL, 0.33 mmol). The mixture was stirred for 4 h and then purified by reverse-phase chromatography (gradient of MeCN/water with 0.1% TFA to provide a diastereomeric mixture, which was then resolved using chiral column chromatography (Chiralpak AD-H column, eluting with 40% MeOH/CO_2) to provide diastereomer 1 (42 mg, 28%) and diastereomer 2 (13 mg, 9%)). Analytical data for the second, more potent diastereomer **3n**: ^{1}H NMR δ (600 MHz, DMSO-d_6) δ 9.10, 9.11 (2 s, 2 H), 8.58 (2 s, 1 H), 5.87 (m, 1 H), 4.33 (m, 2 H), 3.56−3.92 (m, 6 H), 3.41 (m, 1 H), 3.20 (m, 1 H), 2.72 (s, 3 H), 1.89−2.36 (m, 5 H), 1.29 (m, 3 H); HRMS (EI) calcd for $C_{21}H_{26}N_7O_3$ $[M + H]^+$, 424.2097; found, 424.2100.

https://doi.org/10.1021/acs.jmedchem.1c00237
J. Med. Chem. 2021, 64, 5137−5156

(S)-(3-((9-Ethyl-8-(2-methylpyrimidin-5-yl)-9H-purin-6-yl)-amino)pyrrolidin-1-yl)(tetrahydro-2H-pyran-4-yl)methanone (**3o**). A solution of (*S*)-9-ethyl-8-(2-methylpyrimidin-5-yl)-*N*-(pyrrolidin-3-yl)-9*H*-purin-6-amine (200 mg, 0.617 mmol), tetrahydro-2*H*-pyran-4-carboxylic acid (120 mg, 0.925 mmol), Hunig's base (0.32 mL, 1.9 mmol), and HATU (258 mg, 0.678 mmol) in DMF (6 mL) was stirred overnight. 3:1 chloroform/IPA and saturated NH_4Cl were added. The products were extracted into 3:1 chloroform/IPA. The combined organic layers were washed with brine, dried ($MgSO_4$), and concentrated. Purification by chromatography on SiO_2 (25−100% 3:1 EtOAc/EtOH with 1% NH_4 in hexanes) gave (*S*)-(3-((9-ethyl-8-(2-methylpyrimidin-5-yl)-9*H*-purin-6-yl)amino)pyrrolidin-1-yl)-(tetrahydro-2*H*-pyran-4-yl)methanone (**3o**; 155 mg, 58% yield) as a white solid. ^{1}H NMR (600 MHz, DMSO-d_6) δ 9.13 and 9.14 (2 s, 2 H), 8.62 (2 s, 1 H), 5.90 (m, 1 H), 4.37 (m, 2 H), 3.76−3.88 (m, 3 H), 3.58−3.70 (m, 2 H), 3.29−3.42 (m, 3 H), 2.75 (s, 3 H), 2.60−2.70 (m, 2 H), 2.18−2.40 (m, 2 H), 1.50−1.65 (m, 4 H), 1.33 (m, 3 H); HRMS (EI) calcd for $C_{22}H_{29}N_8O_2$ $[M + H]^+$ 437.2413; found 437.2413.

(S)-(3-((9-Ethyl-8-(2-methylpyrimidin-5-yl)-9H-purin-6-yl)oxy)-pyrrolidin-1-yl)(tetrahydro-2H-pyran-4-yl)methanone (**3p**). A solution of (*S*)-9-ethyl-8-(2-methylpyrimidin-5-yl)-6-(pyrrolidin-3-yloxy)-9*H*-purine, 2HCl (35 mg, 0.088 mmol) in DMF (1 mL) was treated with Hunig's base (0.10 mL, 0.57 mmol) followed by tetrahydro-2*H*-pyran-4-carbonyl chloride (15 mg, 0.10 mmol), stirred for 1 h, filtered, and purified by reverse-phase chromatography (gradient of MeCN/water with 0.1% TFA) to provide the TFA salt of **3p** (19 mg, 32%). ^{1}H NMR (600 MHz, CD_3OD) δ 9.09 (s, 2 H), 8.57 (m, 1 H), 6.00 (m, 1 H), 4.41 (m, 2 H), 3.70−4.06 (m, 6 H), 3.39−3.50 (m, 2 H), 2.83 (m, 1 H), 2.80 (s, 3 H), 2.75 (m, 1 H), 2.29−2.45 (m, 2 H), 1.70−1.78 (m, 2 H), 1.63−1.68 (m, 2 H), 1.43 (m, 3 H); HRMS (EI) calcd for $C_{22}H_{28}N_7O_3$ $[M + H]^+$ 438.2254; found 438.2261.

(S)-(3-((9-Ethyl-8-(2-methylpyrimidin-5-yl)-9H-purin-6-yl)-amino)pyrrolidin-1-yl)(oxazol-4-yl)methanone (**3q**). Compound **3q** was prepared via a sequence analogous to that used for the synthesis of **3e**. MS (EI) calcd for $C_{20}H_{22}N_9O_2$ $[M + H]^+$ 420; found 420.

(S)-(3-((9-Ethyl-8-(2-methylpyrimidin-5-yl)-9H-purin-6-yl)oxy)-pyrrolidin-1-yl)(oxazol-4-yl)methanone (**3r**). A mixture of (*S*)-9-ethyl-8-(2-methylpyrimidin-5-yl)-6-(pyrrolidin-3-yloxy)-9*H*-purine (137 mg, 0.421 mmol), oxazole-4-carboxylic acid (48 mg, 0.42 mmol), and HATU (176 mg, 0.463 mmol) in DMF (3.5 mL) was treated with Hunig's base (0.22 mL, 1.3 mmol). The mixture was stirred for 16 h, diluted with EtOAc and sat'd NH_4Cl, extracted with EtOAc, dried (Na_2SO_4), filtered, and concentrated. Chromatography on SiO_2 (0−7% MeOH/DCM) gave the desired product **3r** (83 mg, 47%): ^{1}H NMR (600 MHz, DMSO-d_6) δ 9.12 and 9.13 (2s, 2 H), 8.64 and 8.66 (2s, 1 H), 8.60 and 8.62 (2s, 1 H), 8.47 and 8.51 (2s, 1 H), 5.93 (m, 1 H), 4.35 (m, 1 H), 4.23 (m, 1 H), 3.58−3.98 (m, 4 H), 2.73 (s, 3 H), 2.24−2.39 (m, 2 H), 1.31 (m, 3 H); HRMS (EI) calcd for $C_{20}H_{21}N_8O_3$ $[M + H]^+$ 421.1737; found 421.1739.

(S)-Cyclopropyl(3-((9-ethyl-8-(6-(trifluoromethyl)pyridin-3-yl)-9H-purin-6-yl)amino)pyrrolidin-1-yl)methanone (**4a**). A mixture of (*S*)-(3-aminopyrrolidin-1-yl)(cyclopropyl)methanone (94 mg, 0.61 mmol), 6-chloro-9-ethyl-8-(6-(trifluoromethyl)pyridin-3-yl)-9*H*-purine (100 mg, 0.31 mmol), and DIEA (0.27 mL, 1.5 mmol) in DMF (2 mL) was stirred overnight at 90 °C. The crude reaction mixture was purified by reverse-phase chromatography (gradient of MeCN/water with 0.1% TFA) to provide 50 mg (37%) of the desired product **4a**. ^{1}H NMR (600 MHz, CD_3OD) δ 9.18 (s, 1 H), 8.48 (s, 1 H), 8.42 (m, 1 H), 8.03 (m, 1 H), 4.40−4.44 (m, 2 H), 4.20 (m, 1 H), 3.80−3.95 (m, 2 H), 3.60−3.65 (m, 1 H), 2.30−2.40 (m, 1 H), 2.10−2.25 (m, 1 H), 1.70−1.85 (m, 2 H), 1.40−1.50 (m, 3 H), 0.78−0.98 (m, 4 H); HRMS (EI) calcd for $C_{21}H_{23}F_3N_7O$ $[M + H]^+$ 446.1916; found 446.1918.

(S)-Cyclopropyl(3-((9-ethyl-8-(6-(trifluoromethyl)pyridin-3-yl)-9H-purin-6-yl)oxy)pyrrolidin-1-yl)methanone (**4b**). Synthesized according to the procedure followed for the synthesis of **4c**. ^{1}H NMR (600 MHz, DMSO-d_6) δ 9.18 (s, 1 H), 8.62 (s, 1 H), 8.55 (m, 1 H), 8.10 (m, 1 H), 5.87 (m, 1 H), 4.35−4.40 (m, 2 H), 3.82−4.05 (m, 2 H), 3.55−3.75 (m, 2 H), 2.25−2.40 (m, 1 H), 2.18−2.25 (m, 1 H), 1.70−1.82 (m, 1 H), 1.30−1.40 (m, 3 H), 0.65−0.75 (m, 4 H); HRMS (EI) calcd for $C_{21}H_{22}F_3N_6O_2$ $[M + H]^+$ 447.1756; found 447.1754.

((S)-3-((9-Ethyl-8-(6-(trifluoromethyl)pyridin-3-yl)-9H-purin-6-yl)-oxy)pyrrolidin-1-yl)((1S,3R)-3-methoxycyclobutyl)methanone (**4c**). A solution of (*S*)-*tert*-butyl-3-hydroxypyrrolidine-1-carboxylate (430 mg, 2.30 mmol) in dioxane (10 mL) was treated with a 60% suspension of NaH (120 mg, 3.00 mmol), stirred for 10 min, then treated with 6-chloro-9-ethyl-8-(6-(trifluoromethyl)pyridin-3-yl)-9*H*-purine (500 mg, 1.53 mmol), stirred at 20 °C for 16 h, diluted with DCM, and washed with water. The organic layer was dried (Na_2SO_4) and concentrated to a colorless oil. Chromatography on SiO_2 (gradient of 0−30% MeOH/DCM) gave the desired intermediate, (*S*)-*tert*-butyl-3-((9-ethyl-8-(6-(trifluoromethyl)pyridin-3-yl)-9*H*-purin-6-yl)oxy)pyrrolidine-1-carboxylate (670 mg, 92% yield) as a colorless oil. ^{1}H NMR (600 MHz, DMSO-d_6) δ 9.18 (s, 1 H), 8.60 (s, 1 H), 8.53 (d, J = 8.0 Hz, 1 H), 8.11 (d, J = 8.1 Hz, 1 H), 5.82 (m, 1 H), 4.36 (q, J = 7.1 Hz, 2 H), 3.59−3.69 (m, 1 H), 3.43−3.51 (m, 2 H), 3.18−3.26 (m, 1 H), 3.30−3.41 (m, 1 H), 2.19−2.25 (m, 1 H), 1.37 (m, 9 H), 1.32 (t, J = 7.2 Hz, 3 H); MS (EI) calcd for $C_{22}H_{26}F_3N_6O_3$ $[M + H]^+$ 479; found 479.

A solution containing (*S*)-*tert*-butyl-3-((9-ethyl-8-(6-(trifluoromethyl)pyridin-3-yl)-9*H*-purin-6-yl)oxy)pyrrolidine-1-carboxylate (670 mg, 1.40 mmol) in DCM (10 mL) was treated with a 4 M solution of HCl in dioxane (1.0 mL, 4.0 mmol). The reaction mixture was stirred for 4 h and then concentrated to dryness to provide the desired product as a white amorphous solid, the HCl salt. MS (EI) calcd for $C_{17}H_{18}F_3N_6O$ $[M + H]^+$ 379; found 379.

A solution of (*S*)-9-ethyl-6-(pyrrolidin-3-yloxy)-8-(6-(trifluoromethyl)pyridin-3-yl)-9*H*-purine, HCl (250 mg, 0.603 mmol) in DMF (3 mL) was treated with Hunig's base (0.30 mL, 1.7 mmol), HATU (300 mg, 0.79 mmol), and finally (1*S*,3*S*)-3-methoxycyclobutanecarboxylic acid (120 mg, 0.922 mmol). The reaction mixture was stirred overnight at 20 °C. The mixture was filtered and purified by reverse-phase chromatography (gradient of MeCN/water with 0.1% NH_4OH) to provide **4c** (150 mg; 51%). $[\alpha]_D$ = +44° (c 0.5, MeOH); ^{1}H NMR (600 MHz, DMSO-d_6) δ 9.17 (s, 1 H), 8.60 (s, 1 H), 8.52 (d, J = 8 Hz, 1 H), 8.11 (d, J = 8 Hz, 1 H), 5.85 (m, 1 H), 4.33−4.39 (m, 2 H), 3.60−3.83 (m, 3 H), 3.54 (m, 1 H), 3.37 (m, 1 H), 3.04, 3.06 (2s, 3 H), 2.75 (m, 1 H), 2.13−2.40 (m, 4 H), 1.85−1.95 (m, 2 H), 1.32 (m, 3 H); ^{13}C NMR (125 MHz, DMSO-d_6) δ 172.0, 159.7, 154.2, 152.3, 150.4, 149.0, 147.7, 139.5, 129.5, 123.0, 121.4, 121.3, 76.2, 70.1, 54.7, 51.9, 44.1, 33.0, 32.7, 31.8, 30.1, 28.6, 15.3; HRMS (EI) calcd for $C_{23}H_{26}F_3N_6O_3$ $[M + H]^+$ 491.2018; found 491.2020.

(S)-(3-((9-Ethyl-8-(6-(trifluoromethyl)pyridin-3-yl)-9H-purin-6-yl)-oxy)pyrrolidin-1-yl)(3-methoxyazetidin-1-yl)methanone (**4d**). A mixture containing (*S*)-pyrrolidin-3-ol (2.0 g, 23 mmol) and 4-nitrophenyl 3-methoxyazetidine-1-carboxylate (6.9 g, 28 mmol) in n-BuOH (57 mL) was heated to 100 °C, stirred for 4 h, diluted with EtOAc, washed with water, dried (Na_2SO_4), and concentrated to provide (*S*)-(3-hydroxypyrrolidin-1-yl)(3-methoxyazetidin-1-yl)-methanone (4.75 g). MS (EI) calcd for $C_9H_{17}N_2O_3$ $[M + H]^+$ 201; found 201.

A solution of (*S*)-(3-hydroxypyrrolidin-1-yl)(3-methoxyazetidin-1-yl)methanone (3.74 g, 18.7 mmol) in 50 mL of THF was treated at 0 °C with a 60% suspension of NaH (934 mg, 23.4 mmol). The mixture was stirred for 5 min and then treated with 6-chloro-9-ethyl-8-(6-(trifluoromethyl)pyridin-3-yl)-9*H*-purine (5.10 g, 15.6 mmol). The reaction mixture was stirred for 2 h, diluted with EtOAc, and washed with water. The organic layer was dried (Na_2SO_4) and concentrated. Chromatography on SiO_2 (gradient of 3−15% MeOH/EtOAc) gave the desired product (*S*)-(3-((9-ethyl-8-(6-(trifluoromethyl)pyridin-3-yl)-9*H*-purin-6-yl)oxy)pyrrolidin-1-yl)(3-methoxyazetidin-1-yl)-methanone **4d** (6.1 g, 80%). $[\alpha]_D$ = +42° (c 0.5, MeOH); ^{1}H NMR (600 MHz, $CDCl_3$) δ 9.10 (s, 1 H), 8.56 (s, 1 H), 8.34 (d, J = 6.5 Hz, 1 H), 7.87 (d, J = 8.1 Hz, 1 H), 5.87 (m, 1 H), 4.41 (q, J = 7.2 Hz, 2 H), 4.06−4.18 (m, 4 H), 3.81−3.92 (m, 3 H), 3.55−3.73 (m, 2 H), 3.26 (s, 3 H), 2.02−2.25 (m, 2 H), 1.49 (d, J = 7.2 Hz, 3 H); ^{13}C

https://doi.org/10.1021/acs.jmedchem.1c00237
J. Med. Chem. 2021, 64, 5137−5156

NMR (150 MHz, DMSO-d_6) δ 160.8, 159.8, 154.2, 152.3, 150.4, 148.9, 147.7, 139.5, 129.5, 122.9, 121.5, 121.4, 121.0, 76.5, 69.2, 57.5, 57.4, 55.7, 52.8, 45.0, 31.2, 15.3; HRMS (EI) calcd for $C_{22}H_{25}F_3N_7O_3$ $[M + H]^+$ 492.1971; found 492.1964.

*((S)-3-((9-Ethyl-8-(6-(trifluoromethyl)pyridin-3-yl)-9H-purin-6-yl)-oxy)pyrrolidin-1-yl)((S or R)-tetrahydrofuran-3-yl)methanone (**4e**).* A solution of (*S*)-9-ethyl-6-(pyrrolidin-3-yloxy)-8-(6-(trifluoromethyl)pyridin-3-yl)-9*H*-purine (500 mg, 1.32 mmol) in dioxane (10 mL) was treated with Hunig's base (0.50 mL, 2.9 mmol), HATU (700 mg, 1.84 mmol), and tetrahydrofuran-3-carboxylic acid (200 mg, 1.72 mmol). The reaction mixture was stirred overnight at 20 °C, then diluted with DCM, and washed with water. The organic layer was dried (Na_2SO_4) and concentrated to dryness. Chromatography on SiO_2 (0−30% MeOH/DCM using 120 g of silica) gave the desired product as a set of diastereomers. The colorless oil (550 mg) was then dissolved in 8 mL of MeOH and resolved using chiral column chromatography (column 21 × 250 mm Chiralpak AD-H; 70 mL/min 30% MeOH/CO_2 with 0.25% Me_2NEt; 0.4 mL per injection) to provide the desired diastereomer (225 mg, t_R = 3.49 min) and undesired diastereomer (275 mg, t_R = 5.15 min). $[\alpha]_D$ = +46° (c 0.5, MeOH); ^{1}H NMR (600 MHz, DMSO-d_6) δ 9.17 (s, 1 H), 8.60 (s, 1 H), 8.52 (m, 1 H), 8.12 (d, J = 8.1 Hz, 1 H), 5.84−5.93 (m, 1 H), 4.36 (m, 2 H), 3.82−3.94 (m, 2 H), 3.74−3.80 (m, 1 H), 3.56−3.73 (m, 2 H), 3.41 (m, 1 H), 3.15−2.25 (m, 2 H), 2.98 (m, 1 H), 2.15−2.37 (m, 2 H), 1.90−2.10 (m, 2 H), 1.32 (2 t, J = 7.2 Hz, 3 H); ^{13}C NMR (150 MHz, DMSO-d_6) δ 171.7, 159.8, 154.2, 152.4, 150.4, 148.9, 147.6, 139.5, 129.5, 122.8, 121.4, 121.0, 76.2, 70.1, 68.2, 52.3, 44.7, 42.5, 31.7, 30.2, 29.9, 15.3; HRMS (EI) calcd for $C_{22}H_{24}F_3N_6O_3$ $[M + H]^+$ 477.1862; found 477.1873.

*(S)-(3-((9-Ethyl-8-(6-(trifluoromethyl)pyridin-3-yl)-9H-purin-6-yl)-oxy)pyrrolidin-1-yl)(oxazol-4-yl)methanone (**4f**).* A solution of (*S*)-9-ethyl-6-(pyrrolidin-3-yloxy)-8-(6-(trifluoromethyl)pyridin-3-yl)-9*H*-purine (250 mg, 0.661 mmol) in DMF (3 mL) was treated with Hunig's base (0.30 mL, 1.7 mmol), HATU (300 mg, 0.789 mmol), and oxazole-4-carboxylic acid (120 mg, 1.06 mmol). The reaction mixture was stirred at 20 °C overnight, filtered, and purified by reverse-phase chromatography (gradient of MeCN/water with 0.1% NH4OH) to provide the desired product. $[\alpha]_D$ = +52° (c 0.5, MeOH); ^{1}H NMR (600 MHz, DMSO-d_6) δ 9.17 (m, 1 H), 8.59−8.65 (m, 2 H), 8.51 (m, 1 H), 8.46 (m, 1 H), 8.10 (m, 1 H), 5.94 (m, 1 H), 4.36 (q, J = 7.1 Hz, 2 H), 4.08−4.26 (m, 2 H), 3.79−3.95 (m, 2 H), 3.75 (m, 1 H), 3.60 (m, 1 H), 2.23−2.42 (m, 2 H), 1.31 (q, J = 7.0 Hz, 3 H); ^{13}C NMR (125 MHz, DMSO-d_6) δ 160.0, 159.8, 154.2, 152.4, 152.3, 150.4, 149.0, 147.8, 144.1, 143.9, 139.5, 136.4, 129.5, 121.4, 121.3, 76.1, 53.5, 45.8, 32.2, 29.4, 15.3; HRMS (EI) calcd for $C_{21}H_{19}F_3N_7O_3$ $[M + H]^+$ 473.1501; found 473.1512.

HTRF PI3K Biochemical Assay. PI3K family biochemical potencies in the phosphorylation of PIP2 (phosphatidylinositol (4,5)-bisphosphate) to PIP3 (phosphatidylinositol (3,4,5)-trisphosphate) were measured using an HTRF assay. PI3K biochemical assays were optimized from an Upstate (Millipore) HTRF kit. Briefly, compounds were serially diluted (3-fold in 100% DMSO) for a 10 concentration dose response. A PI3K reaction buffer was prepared by dilution of stock with DI water and then treated with DTT, PIP2, and biotin-PIP3 at final concentrations of 5 μM, 5 μM and 25 nM, respectively. Enzyme and the compounds were added at RT for a 15 min preincubation. Reactions were initiated by addition of substrate solution (PIP2 and ATP) and incubated at RT for 1 h before quenching with EDTA. The detection solution (streptavidin-APC with Eu-labeled anti-GST plus GST-tagged PH-domain) was added and incubated in the dark for 1 h followed by measurement of the HTRF signal with an Envision plate reader (330 nm excitation and dual emission detection at 620 nm (Eu) and 665 nm (APC)). The individual kinases were purchased from Upstate (PI3Kα 14-602, PI3Kβ 14-603, PI3Kγ 14-558, and PI3Kδ 14-604). The assay format was the same for all four isoforms, and the differences lie in the concentration of enzyme and ATP used. The PI3Kα, PI3Kβ, PI3Kδ, and PI3Kγ assays were run with 0.5, 1, 0.3, and 5 nM of enzyme, respectively. The ATP concentration was 100 μM in the PI3Kα, PI3Kβ, and PI3Kδ assays and 50 μM in the PI3Kγ assay.

Ramos AKT-pSer473 Assay. The phosphorylation status of serine 473 of AKT in the Ramos lymphoma-derived B cell line is driven by PI3Kδ, hence a good measure of cellular activity of PI3Kδ inhibition. The Ramos cell line expresses cell surface IgM and responds to IgM cross-linking by activating PI3Kδ-dependent signaling. The AlphaScreen SureFire Akt p-Ser473 assay was used to measure the phosphorylation of endogenous AKT in cellular lysates. B lymphocyte Ramos cells (ATCC catalog #CRL-1596) were split 1:3 every 3 to 4 days and maintained between 100,000 and 1,000,000 cells/mL. Cells were diluted in assay media (DMEM, high glucose, HEPES, No phenol red supplemented with sodium pyruvate) to a concentration of 10,000,000 cells/mL and plated (6 μL, 60,000 cells per well) using a BioRaptor. Compounds were serially diluted (3-fold in 100% DMSO) for a 10 concentration dose response, and 10 nL was added to the wells. The mixture was preincubated for 20 min at RT. Anti-IgM (2 μL of 1 μg/mL) was then added, and the plates were incubated at 37 °C for 30 min. The cells were then treated with lysis buffer (2 μL of 5×) and incubated for 30 min at RT. In the dark, acceptor beads (8 μL of 0.039 mg/mL) were added with Ser473 reaction buffer and the plates were incubated for 2 h. Donor beads (3 μL of 0.036 mg/mL) were added in the dark and again incubated for 2 h. The plates were then read on an Envision plate reader.

SKBr3 AKT-pThr308 Assay. The phosphorylation status of threonine 308 of AKT in the breast cancer cell line SKBR3 is driven by PI3Kα, hence a good measure of cellular activity of PI3Kα inhibition. The protocol is identical to that used in the Ramos AKT-pSer473 assay, with the following modifications. SKBR3 cells are used and are stimulated instead by heregulin (2 μL of 0.05 μg/mL). In addition, Thr308 reaction buffer was used with the acceptor beads.

Human Whole Blood B-Cell Activation CD69 Biomarker Assay. B cell activation is linked to a broad number of diseases including oncology, arthritis, and lupus. Activation of B-cells can be induced ex vivo by stimulation with antibodies that recognize components of the B-cell receptor. These antibodies cross-link receptors on the surface of the B cell, inducing a receptor signaling cascade that drives cell activation. The B-cell receptor is composed of three subunits: a transmembrane IgM for antigen recognition, and CD79a and CD79b, with small cell surface epitopes and prominent intracellular domains containing ITAM signaling subunits. Human whole blood was obtained from healthy volunteer donors at Merck & Co., Inc., Kenilworth, NJ, USA. Using an Echo liquid handler, 120 nL of the compound in DMSO at varying concentrations in a 96-well plate was then treated with 100 μL of blood and incubated for 60 min at 37 °C. To each well was added 11 μL of anti-CD76b antibody (BD Biosciences), and the mixture was incubated for 3 h at 37 °C. The reaction was stopped by placing on wet ice for 5 min. Each well was treated with 50 μL of staining cocktail (CD45-V450, 5 μL; CD3-APC, 5 μL; CD20-PerCP-Cy5-5, 7.5 μL; CD69-FITC, 20 μL in FACS Buffer, 12.5 μL; all from BD Biosciences). The mixture was incubated for 30 min at 4 °C. The red blood cells were lysed by the addition of 1.8 mL of FACS lysis buffer to each well, followed by incubation for 20 min at 20 °C. The plate containing the cells was spun at a rate of 1000 rpm for 5 min, the resulting supernatant was removed, and an aborbent pad was used to collect any excess liquid. The pellet was resuspended in each well in 250 μL of FACS reading buffer (1× BD stain buffer, 0.5% Pluronic F68, 0.2 mg/mL human IgG), and cells were transferred to a clean 384 well U-bottom Greiner plate. Fixed and stained cells are kept at 4 °C before analyzing fluorescence with a Fortessa A FACS machine. Gating: Gate1 = Lymphocyte, based on CD45 and side scatter; Gate2 = Singlet (from gate1), based on forward scatter A&H; Gate3 = B cell (from gate2), which are CD3-APC negative and CD20-PerCP Cy5.5 positive; Gate4 = Activated B cell (from gate3), which are CD69-FITC positive.

Human Whole Blood Basophil Activation CD63 Biomarker Assay. Basophils are the least common leukocyte but are an important effector cell population in allergy, with CD63 being one of the best described biomarkers of basophil activation. Human whole blood was obtained from healthy volunteer donors at Merck & Co., Inc., Kenilworth, NJ, USA. Using an Echo liquid handler, 120 nL of the compound in DMSO at varying concentrations was then treated

https://doi.org/10.1021/acs.jmedchem.1c00237
J. Med. Chem. 2021, 64, 5137−5156

with 100 μL of blood and incubated for 30 min at 37 °C. To each well was added 20 μL of reagent B (Basotest kit; Gylcotope Biotechnology, cat#10-0500), and the mixture was incubated for 30 min at 37 °C. Separately, basophil cell activating goat anti-human IgE antibodies (0.7 μL; Bethyl Laboratories) were prepared to a final concentration of 50 ng/mL in reagent A (200 μL; also from Basotest kit). Each well was treated with 10 μL of the activating anti-IgE, and the plates were incubated for 20 min at 37 °C. The reaction was stopped by placing on wet ice for 5 min. Each well was treated with 30 μL of reagent F stain (anti-human CD63-FITC and anti-human IgE-PE reagent solution; 10 mL, anti-human CD203c-APC; 1500 μL, anti-human CD45-V450; 313 μL, in FACS dilution buffer; 5 mL). The mixture was incubated for 20 min at 4 °C. The red blood cells were lysed by the addition of 1.9 mL of FACS lysis buffer to each well, followed by incubation for 15 min at 20 °C. The plates were spun at 1500 rpm for 5 min, and the supernatant aspirated. The pellet was suspended in 70 μL of FACS reading buffer (1× phosphate buffered saline, 0.2% bovine serum albumin, 0.5% pluronic F-68, 0.2 mg/mL human IgG) and the plate maintained at 4 °C. Plates were read using LSR Fortessa flow cytometer. An anti-human IgE gate was used to count basophil cells, and a CD63+ gate was used to analyze for activated basophil cells. The IC_{50} values were calculated from percent inhibition values of CD63 activated basophils using ADA software to fit to a sigmoidal dose response.

HeLa Cell Adenosine Uptake (AdU) Inhibition Assay. Dilution plates with the compound in DMSO were prepared as a 10-point titration and diluted with HBSS with 5% FBS to reach concentrations of 25,000 to 0.8 nM of the compound. HeLa cells (ATCC) were thawed and seeded at 25,000 cells/well in Cytostar T plates overnight in MEM and 10% FBS. The growth media were removed by flicking, 40 μL of HBSS with 5% FBS was added, and then 40 μL of the compound in buffer was added to the cells. The solution was incubated for 30 min. 20 μL of radiolabeled 100 nM 3*H*-adenosine (ARC; 40 Ci/mmol specific activity and 1 mCi/mL concentration from 25,000 nM stock concentration) in HBSS with 5% FBS was added, and the solution was incubated for 60 min. A total volume of 100 μL was reached, with compound concentrations of 10,000 to 0.32 nM. To measure the uptake of radioactive adenosine, plates were read with a PerkinElmer TopCount NXT HTS plate reader. Data was analyzed using ADA Logic to fit to a 4-parameter fit to provide IC_{50} values.

■ ASSOCIATED CONTENT

Supporting Information

The Supporting Information is available free of charge at https://pubs.acs.org/doi/10.1021/acs.jmedchem.1c00237.

Substitution about the pyrrolidine cyclopropane amide selectivity motif of **3c**, crystallographic data collection and refinement statistics for **3c**, molecular formula strings, and purity HPLC traces for lead compounds (PDF)

Crystallographic data of **3c** (CSV)

Accession Codes

Accession codes have been deposited in the RCSB Protein Data Bank; Compound **3c** (MSD-496486311) ID: 7LM2.

■ AUTHOR INFORMATION

Corresponding Author

Joey L. Methot − *Discovery Chemistry, Merck & Co., Inc., Boston, Massachusetts 02115, United States;* orcid.org/0000-0003-3374-181X; Email: joey_methot@merck.com

Authors

Hua Zhou − *Discovery Chemistry, Merck & Co., Inc., Boston, Massachusetts 02115, United States*

Meredeth A. McGowan − *Discovery Chemistry, Merck & Co., Inc., Boston, Massachusetts 02115, United States*

Neville John Anthony − *Discovery Chemistry, Merck & Co., Inc., Boston, Massachusetts 02115, United States*

Matthew Christopher − *Discovery Chemistry, Merck & Co., Inc., Boston, Massachusetts 02115, United States*

Yudith Garcia − *Discovery Chemistry, Merck & Co., Inc., Boston, Massachusetts 02115, United States*

Abdelghani Achab − *Discovery Chemistry, Merck & Co., Inc., Boston, Massachusetts 02115, United States*

Kathryn Lipford − *Discovery Chemistry, Merck & Co., Inc., Boston, Massachusetts 02115, United States*

Benjamin Wesley Trotter − *Discovery Chemistry, Merck & Co., Inc., Boston, Massachusetts 02115, United States;* orcid.org/0000-0002-6780-0358

Michael D. Altman − *Computational and Structural Chemistry, Merck & Co., Inc., Boston, Massachusetts 02115, United States*

Xavier Fradera − *Discovery Chemistry, Merck & Co., Inc., Boston, Massachusetts 02115, United States;* orcid.org/0000-0002-6118-075X

Charles A. Lesburg − *Discovery Chemistry, Merck & Co., Inc., Boston, Massachusetts 02115, United States;* orcid.org/0000-0001-7245-7331

Chaomin Li − *Process Chemistry, Merck & Co., Inc., Boston, Massachusetts 02115, United States*

Stephen Alves − *Discovery Biology, Merck & Co., Inc., Boston, Massachusetts 02115, United States*

Craig P. Chappell − *Discovery Biology, Merck & Co., Inc., Boston, Massachusetts 02115, United States*

Renu Jain − *Discovery Biology, Merck & Co., Inc., Boston, Massachusetts 02115, United States*

Ruban Mangado − *Discovery Biology, Merck & Co., Inc., Boston, Massachusetts 02115, United States*

Elaine Pinheiro − *Discovery Biology, Merck & Co., Inc., Boston, Massachusetts 02115, United States*

Sybill M. G. Williams − *Discovery Biology, Merck & Co., Inc., Boston, Massachusetts 02115, United States*

Peter Goldenblatt − *In Vitro Pharmacology, Merck & Co., Inc., Boston, Massachusetts 02115, United States*

Armetta Hill − *In Vitro Pharmacology, Merck & Co., Inc., Boston, Massachusetts 02115, United States*

Lynsey Shaffer − *In Vitro Pharmacology, Merck & Co., Inc., Boston, Massachusetts 02115, United States*

Dapeng Chen − *Preclinical Pharmacokinetics and Drug Metabolism, Merck & Co., Inc., Boston, Massachusetts 02115, United States*

Vincent Tong − *Preclinical Pharmacokinetics and Drug Metabolism, Merck & Co., Inc., Boston, Massachusetts 02115, United States*

Robbie L. McLeod − *In Vivo Pharmacology, Merck & Co., Inc., Boston, Massachusetts 02115, United States*

Hyun-Hee Lee − *In Vivo Pharmacology, Merck & Co., Inc., Boston, Massachusetts 02115, United States*

Hongshi Yu − *Discovery Pharmaceutical Sciences, Merck & Co., Inc., Boston, Massachusetts 02115, United States*

Sanjiv Shah − *In Vitro Pharmacology, Merck & Co., Inc., Boston, Massachusetts 02115, United States*

Jason D. Katz − *Discovery Chemistry, Merck & Co., Inc., Boston, Massachusetts 02115, United States*

Complete contact information is available at: https://pubs.acs.org/10.1021/acs.jmedchem.1c00237

https://doi.org/10.1021/acs.jmedchem.1c00237
J. Med. Chem. 2021, 64, 5137−5156

Notes

The authors declare no competing financial interest.

■ ACKNOWLEDGMENTS

The authors would like to thank Dr. Scott K. Pruitt and Peter Fuller for assistance in preparing this manuscript.

■ REFERENCES

(1) (a) Di Paolo, G.; De Camilli, P. Phosphoinositides in Cell Regulation and Membrane Dynamics. *Nature* **2006**, *443*, 651−657. (b) Hawkins, P. T.; Anderson, K. E.; Davidson, K.; Stephens, L. R. Signalling Through Class I PI3Ks in Mammalian Cells. *Biochem. Soc. Trans.* **2006**, *34*, 647−662.

(2) (a) Macias-Perez, I. M.; Flinn, I. W. GS-1101: A Delta-Specific PI3K Inhibitor in Chronic Lymphocytic Leukemia. *Curr. Hematol. Malig. Rep.* **2013**, *8*, 22−27. (b) Fruman, D. A.; Rommel, C. PI3K and Cancer: Lessons, Challenges and Opportunities. *Nat. Rev. Drug Discovery* **2014**, *13*, 140−156. (c) Wei, M.; Wang, X.; Song, Z.; Jiao, M.; Ding, J.; Meng, L.-H.; Zhang, A. Targeting PI3Kδ: Emerging Therapy for Chronic Lymphocytic Leukemia and Beyond. *Med. Res. Rev.* **2015**, *35*, 720−752. (d) Thorpe, L. M.; Yuzugullu, H.; Zhao, J. J. PI3K in Cancer: Divergent Roles of Isoforms, Modes of Activation and Therapeutic Targeting. *Nat. Rev. Cancer* **2015**, *15*, 7−24. (e) *Zydelig, by* Gilead Sciences, Inc.. https://www.zydelig.com/index.aspx; (f) Yang, Q.; Modi, P.; Newcomb, T.; Quéva, C.; Gandhi, V. Idelalisib: First-in-Class PI3K Delta Inhibitor for the Treatment of Chronic Lymphocytic Leukemia, Small Lymphocytic Leukemia, and Follicular Lymphoma. *Clin. Cancer Res.* **2015**, *21*, 1537−1542. (g) Bange, E.; Nabhan, C.; Brander, D. M.; Lamanna, N.; Ujjani, C. S.; Howlett, C.; Skarbnik, A. P.; Hill, B. T.; Cheson, B. D.; Zent, C. S.; Pu, J. J.; Winter, A. M.; Isaac, K.; Kennard, K.; Timlin, C.; Dorsey, C.; Dwivedy Nasta, S.; Svoboda, J.; Landsburg, D. J.; Schuster, S. J.; Barr, P. M.; Mato, A. R. Real-World Evidence for Durable Treatment Responses after Toxicity Related Discontinuation of Idelalisib. *Blood* **2017**, *130*, 4325.

(3) U.S. Food and Drug Administration *Full prescribing information: COPIKTRA (duvelisib) (PDF)*; U.S Food and Drug Administration Retrieved 23 October 2018. https://www.accessdata.fda.gov/drugsatfda_docs/label/2018/211155s000lbl.pdf.

(4) (a) Ali, K.; Soond, D. R.; Piñeiro, R.; Hagemann, T.; Pearce, W.; Lim, E. L.; Bouabe, H.; Scudamore, C. L.; Hancox, T.; Maecker, H.; Friedman, L.; Turner, M.; Okkenhaug, K.; Vanhaesebroeck, B. Inactivation of PI(3)K p110δ breaks regulatory T-cell-mediated immune tolerance to cancer. *Nature* **2014**, *510*, 407−411. (b) Hirsch, E.; Novelli, F. Natural-Born Killers Unleashed. *Nature* **2014**, *510*, 342−343.

(5) (a) Hawkins, P. T.; Stephens, L. R. PI3K Signalling in Inflammation. *Biochim. Biophys. Acta* **2015**, *1851*, 882−897. (b) Stark, A.-K.; Sriskantharajah, S.; Hessel, E. M.; Okkenhaug, K. PI3K Inhibitors in Inflammation, Autoimmunity and Cancer. *Curr. Opin. Pharmacol.* **2015**, *23*, 82−91. (c) Sriskantharajah, S.; Hamblin, N.; Worsley, S.; Calver, A. R.; Hessel, E. M.; Amour, A. Targeting Phosphoinositide 3-Kinase δ for the Treatment of Respiratory Diseases. *Ann. N. Y. Acad. Sci.* **2013**, *1280*, 35−39.

(6) (a) Condliffe, A. M.; Chandra, A. Respiratory Manifestations of the Activated Phosphoinositide 3-Kinase delta Syndrome. *Front. Immunol.* **2018**, *9*, 338. (b) Michalovich, D.; Nejentsev, S. Activated PI3 Kinase Delta Syndrome: From Genetics to Therapy. *Front. Immunol.* **2018**, *9*, 369.

(7) Horak, F.; Puri, K. D.; Steiner, B. H.; Holes, L.; Xing, G.; Zieglmayer, P.; Zieglmayer, R.; Lemell, P.; Yu, A. Randomized Phase 1 Study of the Phosphatidylinositol 3-Kinase δ Inhibitor Idelalisib in Patients with Allergic Rhinitis. *J. Allergy Clin. Immunol.* **2016**, *137*, 1733.

(8) Recent Reviews: (a) Cushing, T. D.; Metz, D. P.; Whittington, D. A.; McGee, L. R. PI3Kδ and PI3Kγ as Targets for Autoimmune and Inflammatory Diseases. *J. Med. Chem.* **2012**, *55*, 8559−8581. (b) Garces, A. E.; Stocks, M. J. Class 1 PI3K Clinical Candidates and Recent Inhibitor Design Strategies: A Medicinal Chemistry Perspective. *J. Med. Chem.* **2019**, *62*, 4815−4850. (c) Perry, M. W. D.; Abdulai, R.; Mogemark, M.; Petersen, J.; Thomas, M. J.; Valastro, B.; Eriksson, A. W. Evolution of PI3Kγ and δ Inhibitors for Inflammatory and Autoimmune Diseases. *J. Med. Chem.* **2019**, *62*, 4783−4814.

(9) (a) Williams, O.; Houseman, B. T.; Kunkel, E. J.; Aizenstein, B.; Hoffman, R.; Knight, Z. A.; Shokat, K. M. Discovery of dual inhibitors of the immune cell PI3Ks p110δ and p110γ: a prototype for new anti-inflammatory drugs. *Chem. Biol.* **2010**, *17*, 123−134. (b) Winkler, D. J.; Faia, K. L.; DiNitto, J. P.; Ali, J. A.; White, K. F.; Brophy, E. E.; Pink, M. M.; Proctor, J. L.; Lussier, J.; Martin, C. M.; Hoyt, J. G.; Tillotson, B.; Murphy, E. L.; Lim, A. R.; Thomas, B. D.; MacDougall, J. R.; Ren, P.; Liu, Y.; Li, L.-S.; Jessen, K. A.; Fritz, C. C.; Dunbar, J. L.; Porter, J. R.; Rommel, C.; Palombella, V. J.; Changelian, P. S.; Kutok, J. L. PI3K-δ and PI3K-γ Inhibition by IPI-145 Abrogates Immune Responses and Suppresses Activity in Autoimmune and Inflammatory Disease Models. *Chem. Biol.* **2013**, *20*, 1364−1374. (c) Cushing, T. D.; Hao, K.; Shin, Y.; Andrews, K.; Brown, M.; Cardozo, M.; Chen, Y.; Duquette, J.; Fisher, B.; Gonzalez-Lopez de Turiso, F.; He, X.; Henne, K. R.; Hu, Y.-L.; Hungate, R.; Johnson, M. G.; Kelly, R. C.; Lucas, B.; McCarter, J. D.; McGee, L. R.; Medina, J. C.; Miguel, T. S.; Mohn, D.; Pattaropong, V.; Pettus, L. H.; Reichelt, A.; Rzasa, R. M.; Seganish, J.; Tasker, A. S.; Wahl, R. C.; Wannberg, S.; Whittington, D. A.; Whoriskey, J.; Yu, G.; Zalameda, L.; Zhang, D.; Metz, D. P. Discovery and in Vivo Evaluation of (*S*)-*N*-(1-(7-Fluoro-2-(pyridin-2-yl)quinolin-3-yl)ethyl)-9*H*-purin-6-amine (AMG319) and Related PI3Kδ Inhibitors for Inflammation and Autoimmune Disease. *J. Med. Chem.* **2015**, *58*, 480−511. (d) Ndubaku, C. O.; Heffron, T. P.; Staben, S. T.; Baumgardner, M.; Blaquiere, N.; Bradley, E.; Bull, R.; Do, S.; Dotson, J.; Dudley, D.; Edgar, K. A.; Friedman, K. S.; Goldsmith, R.; Heald, R. A.; Kolesnikov, A.; Lee, L.; Lewis, C.; Nannini, M.; Nonomiya, J.; Pang, J.; Price, S.; Prior, W. W.; Salphati, L.; Sideris, S.; Wallin, J. J.; Wang, L.; Wei, B.; Sampath, D.; Olivero, A. G. Discovery of 2-{3-[2-(1-Isopropyl-3-methyl-1H-1,2−4-triazol-5-yl)-5,6-dihydrobenzo[f]imidazo[1,2-d][1,4]oxazepin-9-yl]-1H-pyrazol-1-yl}-2-methylpropanamide (GDC-0032): A β-Sparing Phosphoinositide 3-Kinase Inhibitor with High Unbound Exposure and Robust in Vivo Antitumor Activity. *J. Med. Chem.* **2013**, *56*, 4597−4610. (e) Down, K.; Amour, A.; Baldwin, I. R.; Cooper, A. W. J.; Deakin, A. M.; Felton, L. M.; Guntrip, S. B.; Hardy, C.; Harrison, Z. A.; Jones, K. L.; Jones, P.; Keeling, S. E.; Le, J.; Livia, S.; Lucas, F.; Lunniss, C. J.; Parr, N. J.; Robinson, E.; Rowland, P.; Smith, S.; Thomas, D. A.; Vitulli, G.; Washio, Y.; Hamblin, J. N. Optimization of Novel Indazoles as Highly Potent and Selective Inhibitors of Phosphoinositide 3-Kinase δ for the Treatment of Respiratory Disease. *J. Med. Chem.* **2015**, *58*, 7381−7399. (f) Hoegenauer, K.; Soldermann, N.; Stauffer, F.; Furet, P.; Graveleau, N.; Smith, A. B.; Hebach, C.; Hollingworth, G. J.; Lewis, I.; Gutmann, S.; Rummel, G.; Knapp, M.; Wolf, R. M.; Blanz, J.; Feifel, R.; Burkhart, C.; Zécri, F. Discovery and Pharmacological Characterization of Novel Quinazoline-Based PI3K Delta-Selective Inhibitors. *ACS Med. Chem. Lett.* **2016**, *7*, 762−767. (g) Liu, Q.; Shi, Q.; Marcoux, D.; Batt, D. G.; Cornelius, L.; Qin, L.-Y.; Ruan, Z.; Neels, J.; Beaudoin-Bertrand, M.; Srivastava, A. S.; Ling, L.; Cherney, R. J.; Gong, H.; Watterson, S. H.; Weigelt, C.; Gillooly, K. M.; McIntyre, K. W.; Xie, J. H.; Obermeier, M. T.; Fura, A.; Sleczka, B.; Stefanski, K.; Fancher, R. M.; Padmanabhan, S.; Thatipamula, R. P.; Kundu, I.; Rajareddy, K.; Smith, R.; Hennan, J. K.; Xing, D.; Fan, J.; Levesque, P. C.; Ruan, Q.; Pitt, S.; Zhang, R.; Pedicord, D.; Pan, J.; Yarde, M.; Lu, H.; Lippy, J.; Goldstine, C.; Skala, S.; Rampulla, R. A.; Mathur, A.; Gupta, A.; Arunachalam, P. N.; Sack, J. S.; Muckelbauer, J. K.; Cvijic, M. E.; Salter-Cid, L. M.; Bhide, R. S.; Poss, M. A.; Hynes, J.; Carter, P. H.; Macor, J. E.; Ruepp, S.; Schieven, G. L.; Tino, J. A. Identification of a Potent, Selective, and Efficacious Phosphatidylinositol 3-Kinase δ (PI3Kδ) Inhibitor for the Treatment of Immunological Disorders. *J. Med. Chem.* **2017**, *60*, 5193−5208. (h) Perry, M. W. D.; Björhall, K.; Bonn, B.; Carlsson, J.; Chen, Y.; Eriksson, A.; Fredlund, L.; Hao, H.'e.; Holden, N. S.; Karabelas, K.; Lindmark, H.; Liu, F.; Pemberton,

https://doi.org/10.1021/acs.jmedchem.1c00237
J. Med. Chem. 2021, 64, 5137−5156

N.; Petersen, J.; Blomqvist, S. R.; Smith, R. W.; Svensson, T.; Terstiege, I.; Tyrchan, C.; Yang, W.; Zhao, S.; Öster, L. Design and Synthesis of Soluble and Cell-Permeable PI3Kδ Inhibitors for Long-Acting Inhaled Administration. *J. Med. Chem.* **2017**, *60*, 5057−5071. (i) Yue, E. W.; Li, Y.-L.; Douty, B.; He, C.; Mei, S.; Wayland, B.; Maduskuie, T.; Falahatpisheh, N.; Sparks, R. B.; Polam, P.; Zhu, W.; Glenn, J.; Feng, H.; Zhang, K.; Li, Y.; He, X.; Katiyar, K.; Covington, M.; Feldman, P.; Shin, N.; Wang, K. H.; Diamond, S.; Li, Y.; Koblish, H. K.; Hall, L.; Scherle, P.; Yeleswaram, S.; Xue, C.-B.; Metcalf, B.; Combs, A. P.; Yao, W. INCB050465 (Parsaclisib), a Novel Next-Generation Inhibitor of Phosphoinositide 3-Kinase Delta (PI3Kδ). *ACS Med. Chem. Lett.* **2019**, 1554−1560.

(10) Methot, J. L.; Zhou, H.; Kattar, S. D.; McGowan, M. A.; Wilson, K.; Garcia, Y.; Deng, Y.; Altman, M.; Fradera, X.; Lesburg, C.; Fischmann, T.; Li, C.; Alves, S.; Shah, S.; Fernandez, R.; Goldenblatt, P.; Hill, A.; Shaffer, L.; Chen, D.; Tong, V.; McLeod, R. L.; Yu, H.; Bass, A.; Kemper, R.; Gatto, N. T.; LaFranco-Scheuch, L.; Trotter, B. W.; Guzi, T.; Katz, J. D. Structure Overhaul Affords a Potent Purine PI3Kδ Inhibitor with Improved Tolerability. *J. Med. Chem.* **2019**, *62*, 4370−4382.

(11) (a) Marzio, R.; Mauël, J.; Betz-Corradin, S. CD69 and Regulation of the Immune Function. *Immunopharmacol. Immunotoxicol.* **1999**, *21*, 565−582. (b) Del Poeta, G.; Del Principe, M. I.; Zucchetto, A.; Luciano, F.; Buccisano, F.; Rossi, F. M.; Bruno, A.; Biagi, A.; Bulian, P.; Maurillo, L.; Neri, B.; Bomben, R.; Simotti, C.; Coletta, A. M.; Bo, M. D.; de Fabritiis, P.; Venditti, A.; Gattei, V.; Amadori, S. CD69 is Independently Prognostic in Chronic Lymphocytic Leukemia: a Comprehensive Clinical and Biological Profiling Study. *Haematologica* **2012**, *97*, 279−287. (c) Montraveta, A.; Lee-Vergés, E.; Roldán, J.; Jiménez, L.; Cabezas, S.; Clot, G.; Pinyol, M.; Xargay-Torrent, S.; Rosich, L.; Arimany-Nardí, C.; Aymerich, M.; Villamor, N.; López-Guillermo, A.; Pérez-Galán, P.; Roué, G.; Pastor-Anglada, M.; Campo, E.; López-Guerra, M.; Colomer, D. CD69 Expression Potentially Predicts Response to Bendamustine and its Modulation by Ibrutinib or Idelalisib Enhances Cytotoxic Effect in Chronic Lymphocytic Leukemia. *Oncotarget* **2016**, *7*, 5507−5520.

(12) Cl_{int} is the *in vivo* intrinsic clearance; where $Cl_{int} = Cl_u[(Q_{hep}\text{-}Cl_p)Q_{hep}]$ and $Cl_u = [100Cl_p/(100\text{-}PPB)]$, Q_{hep} = 84 mL/min/kg in rat and 30 mL/min/kg in dog.

(13) Meester, B. J.; Shankley, N. P.; Welsh, N. J.; Meijler, F. L.; Black, J. W. Pharmacological Analysis of the Activity of the Adenosine Uptake Inhibitor, Dipyridamole, on the Sinoatrial and Atrioventricular Nodes of the Guinea-pig. *Br. J. Pharmacol.* **1998**, *124*, 729−741.

(14) (a) Achab, A.; Altman, M. D.; Deng, Y.; Guzi, T.; Kattar, S.; Katz, J. D.; Methot, J. L.; Zhou, H.; McGowan, M.; Christopher, M. P.; Garcia, Y.; Anthony, N. J.; Fradera, X.; Mu, C.; Zhang, S.; Zhang, R.; Fong, K. C.; Leng, X. Purine Inhibitors of Human Phosphatidylinositol 3-Kinase Delta. PCT Int. Appl. (2014), WO 2014075392 A1 (b) Achab, A.; Altman, M. D.; Deng, Y.; Kattar, S.; Katz, J. D.; Methot, J. L.; Zhou, H.; McGowan, M.; Christopher, M. P.; Garcia, Y.; Anthony, N. J.; Fradera, X.; Yang, L.; Mu, C.; Wang, X.; Shi, F.; Ye, B.; Zhang, S.; Zhao, X.; Zhang, R.; Fong, K. C.; Leng, X. Purine Inhibitors of Human Phosphatidylinositol 3-Kinase Delta. PCT Int. Appl. (2014), WO 2014075393 A1.

(15) (a) Tang, H.; Mayersohn, M. A Novel Model for Prediction of Human Drug Clearance by Allometric Scaling. *Drug Metab Dispos.* **2005**, *33*, 1297. (b) Sharma, V.; McNeill, J. H. To Scale or Not to Scale: The Principles of Dose Extrapolation. *Br. J. Pharmacol.* **2009**, *157*, 907.

(16) (a) Vignali, D. A. A.; Collison, L. W.; Workman, C. J. How Regulatory T Cells Work. *Nat. Rev. Immunol.* **2008**, *8*, 523−532. (b) Liston, A.; Gray, D. H. D. Homeostatic Control of Regulatory T Cell Diversity. *Nat. Rev. Immunol.* **2014**, *14*, 154−165. (c) Nishikawa, H.; Sakaguchi, S. Regulatory T Cells in Cancer Immunotherapy. *Curr. Opin. Immunol.* **2014**, *27*, 1−7. (c) Adams, J. L.; Smothers, J.; Srinivasan, R.; Hoos, A. Big Opportunities for Small Molecules in Immuno-oncology. *Nat. Rev. Drug Discovery* **2015**, *14*, 603−622. (d) Wolf, D.; Sopper, S.; Pircher, A.; Gastl, G.; Wolf, A. M. Treg(s) in Cancer: Friends or Foe? *J. Cell. Physiol.* **2015**, *230*, 2598−2605.

(17) Luo, C. T.; Liao, W.; Dadi, S.; Toure, A.; Li, M. O. Graded Foxo1 Activity in T_{reg} Cells Differentiates Tumour Immunity from Spontaneous Autoimmunity. *Nature* **2016**, *529*, 532.

(18) (a) Davis, R. J.; Moore, E. C.; Clavijo, P. E.; Friedman, J.; Cash, H.; Chen, Z.; Silvin, C.; Van Waes, C.; Allen, C. Anti-PD-L1 Efficacy Can Be Enhanced by Inhibition of Myeloid-Derived Suppressor Cells with a Selective Inhibitor of PI3Kδ/γ. *Cancer Res.* **2017**, *77*, 2607−2619. (b) Pachter, J. A.; Weaver, D. T. The Dual PI3K-δ,γ Inhibitor Duvelisib Stimulates Anti-Tumor Immunity and Enhances Efficacy of Immune Checkpoint and Co-Stimulatory Antibodies in a B Cell Lymphoma Model. *Blood* **2017**, *130*, 1541. (c) Chellappa, S.; Kushekhar, K.; Munthe, L. A.; Tjønnfjord, G. E.; Aandahl, E. M.; Okkenhaug, K.; Taskén, K. The PI3K p110δ Isoform Inhibitor Idelalisib Preferentially Inhibits Human Regulatory T Cell Function. *J. Immunol.* **2019**, *202*, 1397.

(19) Wan, Y. Y.; Flavell, R. A. Identifying Foxp3-Expressing Suppressor T Cells with a Bicistronic Reporter. *Proc. Natl. Acad. Sci. U. S. A.* **2005**, *102*, 5126.

(20) McLeod, R. L.; Gil, M. A.; Chen, D.; Cabal, A.; Katz, J.; Methot, J.; Woodhouse, J. D.; Dorosh, L.; Geda, P.; Mehta, K.; Cicmil, M.; Baltus, G. A.; Bass, A.; Houshyar, H.; Caniga, M.; Yu, H.; Gervais, F.; Alves, S.; Shah, S. Characterizing Pharmacokinetic−Pharmacodynamic Relationships and Efficacy of $PI_3K\delta$Inhibitors in Respiratory Models of TH_2 and TH_1 Inflammation. *J. Pharmacol. Exp. Ther.* **2019**, *369*, 223.

https://doi.org/10.1021/acs.jmedchem.1c00237
J. Med. Chem. 2021, 64, 5137−5156